

## Measuring Oscillations with a Million Atmospheric Neutrinos

C. A. Argüelles<sup>1,\*</sup>, P. Fernández<sup>2,3,†</sup>, I. Martínez-Soler<sup>1,‡</sup> and M. Jin (靳淼辰)<sup>1,§</sup>

<sup>1</sup>*Department of Physics and Laboratory for Particle Physics and Cosmology, Harvard University, Cambridge, Massachusetts 02138, USA*

<sup>2</sup>*University of Liverpool, Department of Physics, Liverpool, United Kingdom*

<sup>3</sup>*Donostia International Physics Center DIPC, San Sebastián/Donostia E-20018, Spain*

 (Received 16 November 2022; revised 28 September 2023; accepted 4 October 2023; published 20 December 2023)

After two decades of measurements, neutrino physics is now advancing into the precision era. With the long-baseline experiments designed to tackle current open questions, a new query arises: Can atmospheric neutrino experiments also play a role? To that end, we analyze the expected sensitivity of current and near-future water(ice)-Cherenkov atmospheric neutrino experiments in the context of standard three-flavor neutrino oscillations. In this first in-depth combined atmospheric neutrino analysis, we analyze the current shared systematic uncertainties arising from the common flux and neutrino-water interactions. We then implement the systematic uncertainties of each experiment in detail and develop the atmospheric neutrino simulations for Super-Kamiokande, with and without neutron-tagging capabilities, IceCube Upgrade, ORCA, and Hyper-Kamiokande detectors. We carefully review the synergies and features of these experiments to examine the potential of a joint analysis of these atmospheric neutrino data in resolving the  $\theta_{23}$  octant at 99% confidence level (CL), and determining the neutrino mass ordering above  $5\sigma$  by 2030. Additionally, we assess the capability to constrain  $\theta_{13}$  and the  $CP$ -violating phase ( $\delta_{CP}$ ) in the leptonic sector independently from reactor and accelerator neutrino data. A combination of the atmospheric neutrino measurements will enhance the sensitivity to a greater extent than the simple sum of individual experiment results reaching more than  $3\sigma$  for some values of  $\delta_{CP}$ . These results will provide vital information for next-generation accelerator neutrino oscillation experiments such as DUNE and Hyper-Kamiokande.

DOI: [10.1103/PhysRevX.13.041055](https://doi.org/10.1103/PhysRevX.13.041055)

Subject Areas: Particles and Fields

### I. INTRODUCTION

Atmospheric neutrinos have played a key role in discovering and understanding neutrino oscillations [1,2]. The first hint of resilient signatures of deviations from the standard model in neutrinos came from a deficit of muon neutrinos in IMB [3] and Kamiokande [4], which were later confirmed by Super-Kamiokande (SuperK) [5]. These anomalies are now known to be due to neutrinos having nonzero, small masses, and the flavor states and mass states being misaligned [6]. This misalignment produces a characteristic neutrino flavor change, often called oscillations due to its periodic behavior in vacuum, and this flavor

change depends on the ratio of the distance from source to detector,  $L$ —called baseline—and the neutrino energy,  $E_\nu$ .

One of the reasons why atmospheric neutrinos are good discovery experiments is that they cover 10 orders of magnitude in the ratio of baseline to energy,  $L/E_\nu$ . The baseline  $L$  covers ranges from 15 to 12 700 km and the neutrino energy ranges from  $\mathcal{O}(10^{-2})$  to  $\mathcal{O}(10^5)$  GeV. This results in a coverage of  $L/E_\nu$  from  $\mathcal{O}(10^{-4})$  to  $\mathcal{O}(10^6)$  km/GeV. This broad range of  $L/E_\nu$  and the fact that atmospheric neutrinos go through the largest amounts of matter [7] have allowed them to be used for measuring neutrino oscillation parameters [8,9] and placing stringent bounds on new neutrino states [10,11], nonstandard neutrino interactions [12–20], space-time symmetries [21], and other physics beyond the standard model [22,23]; see Fig. 1 for an artistic illustration of atmospheric neutrinos and the detectors used to observe them.

In the last two decades, the neutrino community has developed a vast program using accelerator, reactor, and solar neutrinos to measure their evolution, leading to the conclusion that atmospheric measurements will not contribute to precision neutrino physics. In this article, we change that paradigm, showing that atmospheric neutrinos will improve our knowledge of some of the largest

\*carguelles@fas.harvard.edu

†pablo.fernandez@dipc.org

‡imartinezsoler@fas.harvard.edu

§miaochenjin@g.harvard.edu

Published by the American Physical Society under the terms of the [Creative Commons Attribution 4.0 International license](https://creativecommons.org/licenses/by/4.0/). Further distribution of this work must maintain attribution to the author(s) and the published article's title, journal citation, and DOI.

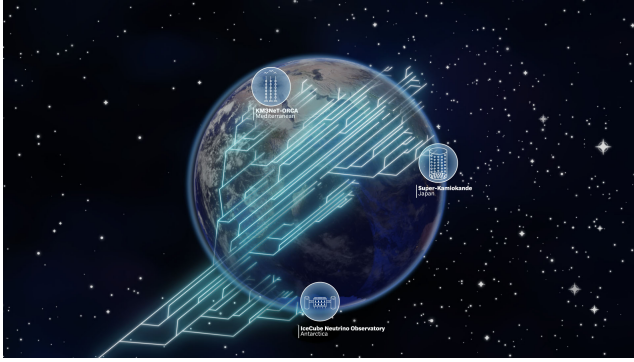


FIG. 1. Illustration of this analysis. Locations of experiments used in this work are shown. Note that Hyper-Kamiokande has roughly the same location as Super-Kamiokande.

unknowns describing the evolution of neutrino states. See Fig. 2 for a comparison between our results, the present status, and the future predictions for the next generation of neutrino experiments. By combining the atmospheric measurements, we aim to achieve the most accurate determination of atmospheric parameters ( $\Delta m_{31}^2$  and  $\theta_{23}$ ). Additionally, this combined approach will yield valuable insights into  $\theta_{13}$  due to the Earth matter effect, as we elaborate upon later. Lastly, the atmospheric measurements are expected to offer a level of precision comparable to current results in determining  $\delta_{CP}$ .

As we demonstrate in this article, data from current and soon-to-operate atmospheric neutrino experiments can be combined to address some of the most pressing questions in neutrino physics. The questions that we discuss in this article can be organized into three categories: determining the neutrino oscillation parameters, establishing the neutrino mass spectra, and measuring the  $CP$  phase in the lepton sector. The neutrino oscillation parameters are encoded in the so-called Pontecorvo-Maki-Nakagawa-Sakata matrix, which relates the neutrino weak and mass eigenstates [30]. The precise determination of the lepton mixing parameters is crucial for understanding the neutrino evolution, and it can also be the first indication of a hidden flavor symmetry [31,32]. Measuring a large  $CP$  violation in the neutrino sector can also be an explanation to the baryon asymmetry of the early Universe via a sphaleron process [33]. Finally, the determination of the neutrino mass spectrum in the next few years will significantly impact experiments whose goal is to determine the absolute scale of the neutrino masses [34], to discriminate between the Dirac or Majorana nature of the neutrino masses [35,36], and even to understand the evolution of the Universe [37].

In the rest of the section, we provide a concise summary of the main results from this study. In atmospheric neutrino oscillations, the dominant mixing angle is  $\theta_{23}$ , and the relevant mass-squared difference is  $\Delta m_{31}^2$ . The atmospheric mixing angle is currently the least precisely determined of the mixing angles and is known to be close to maximal,

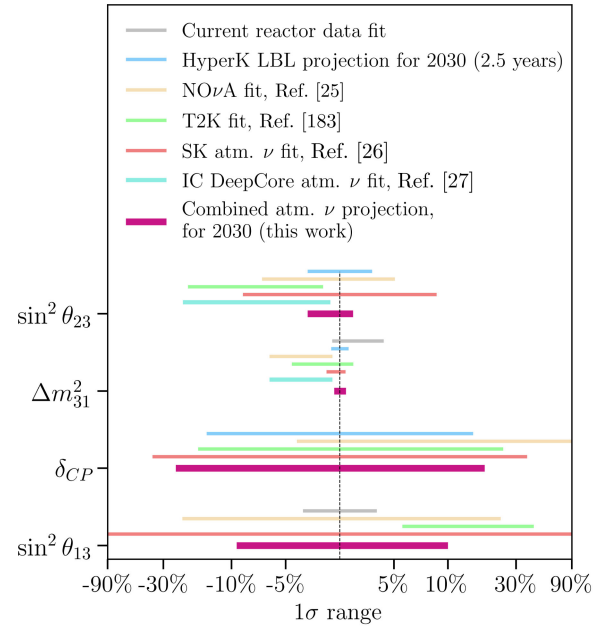


FIG. 2. Comparison between the present and future projected sensitivities for the oscillation parameters. This figure showcases the power of atmospheric combined neutrino experiments, as they have smaller or comparable errors on these parameters than accelerator neutrino experiments also shown in this figure. Oscillation parameters that can be measured by atmospheric experiments are arranged in the vertical axis, while their measured precision is quantified in the horizontal axis. The present ( $1\sigma$ ) region allowed by fit to data from T2K [24] (green), NO $\nu$ A [25] (light orange), SuperK atmospheric neutrinos [26] (light red), DeepCore atmospheric neutrinos [27] (turquoise), the reactor experiments (gray), and the projected sensitivity of Hyper-Kamiokande’s accelerator program (blue) for 2030 [28] is compared with the expected ( $1\sigma$ ) region from a combined atmospheric neutrino analysis (this work in red-violet). The sensitivity from DUNE is excluded due to the low significance achievable by this experiment for 2030 assuming a 2029 starting date [29].

i.e.,  $\sin^2 2\theta_{23} \approx 1$ . However, current experimental data point toward deviations from maximality, but are unable to resolve the octant, i.e., whether  $\theta_{23}$  is smaller or greater than  $\pi/4$ . In terms of the neutrino flavor structure, the maximality and octant question can be rephrased as understanding the relative contribution of tau and muon flavor in the second mass state, where a maximal angle implies equal amounts, the first octant more muon, and the second octant less muon. Therefore, the large muon-neutrino component of the atmospheric flux can provide significant knowledge on that parameter. In this article, we demonstrate that by combining the SuperK, IceCube Upgrade, ORCA, and Hyper-Kamiokande (HyperK) measurements (see Sec. VI), we reach a half-percent-level precision on  $\Delta m_{31}^2$  and approximately 2% in the case of  $\sin^2 \theta_{23}$ ; see Fig. 2. Furthermore, the atmospheric measurements allow us to discriminate the wrong octant at more than  $3\sigma$  by 2030

assuming the current best-fit value of  $\theta_{23}$ ; see Fig. 18. As we discuss in Sec. VIII, those measurements are primarily limited by statistics. In the Supplemental Material [38], we check that our main results and conclusions are independent of the benchmark scenario considered.

The neutrino mass spectra enter the neutrino oscillation expressions through the sign of the mass-squared differences. The neutrino mass states are conventionally labeled by their decreasing number of electron-neutrino components, where  $\nu_1$  is the state that has the most electron neutrinos and  $\nu_3$  the least; in symbols,  $|U_{e1}| > |U_{e2}| > |U_{e3}|$ . From solar neutrino oscillations, it is known that the second mass state  $\nu_2$  is heavier than the first one  $\nu_1$ ; however, it is not known if  $\nu_3$  is heavier (normal ordering, NO) or lighter (abnormal or inverted ordering, IO) than the other two states. This is referred to as the neutrino ordering problem and is one of the main objectives of JUNO [39] and next-generation neutrino experiments DUNE [40] and Hyper-Kamiokande [28]. Currently, the combination of neutrino data favors normal ordering mildly, although no conclusive measurement of this has been achieved to date. In this article, we show that the combination of neutrino experiments discussed in this work determine the neutrino ordering at more than  $5\sigma$  [41]. Atmospheric neutrino experiments can reach  $4\sigma$  sensitivity before the next generation of neutrino accelerator experiments starts taking data; Fig. 3. The sensitivity to this parameter is mainly affected by statistics and the misreconstruction of  $\nu_\tau$  interaction represented by the  $\nu_\tau$  cross section as discussed in Sec. VIII. In Sec. III, we summarize the status of the neutrino cross-section measurements along with the most relevant experimental measurement that will happen in the next year and will contribute to increasing the sensitivity over that parameter.

Finally, we turn to the question of  $CP$  violation in the leptonic sector, which has been previously discussed in the context of atmospheric neutrino experiments [45]. The combination of the experiments considered in this work provides a measurement of the  $CP$ -violating phase that shrinks the allowed region in a factor of 5 (Fig. 2), assuming the preferred value of T2K [46] and SuperK [43,47] measurements, being able to exclude more than half of the allowed parameter space at more than 90% CL for any value of  $\delta_{CP}$ : see Sec. VII. The capacity to measure the  $CP$  phase is dominated by SuperK and HyperK due to their large low-energy neutrino efficiency and neutrino-antineutrino separation ability. The improved neutrino-antineutrino separation is due to a recent upgrade of SuperK, where the detector is doped with gadolinium (SKGd). See Sec. VI for a detailed description of the detector response and the simulation used in this analysis. The combination of a precision measurement of the oscillation parameters by the neutrino telescopes and an improved SuperK detector allows us to bring new and complementary information on the  $CP$  phase compared to that obtained by long-baseline experiments. This is of

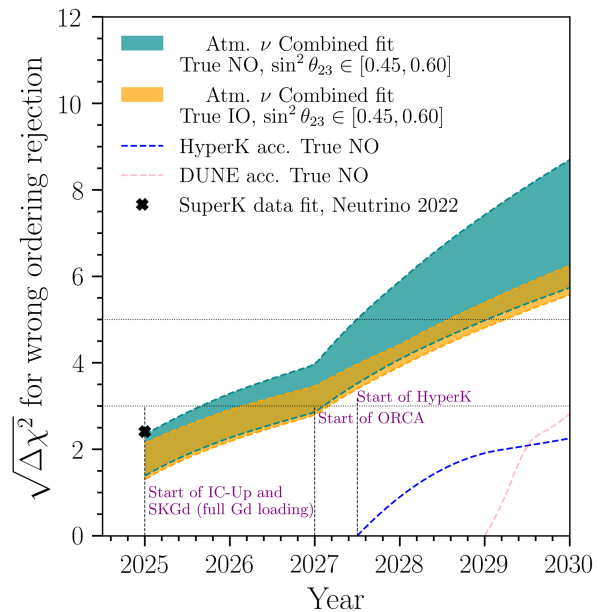


FIG. 3. Neutrino mass ordering sensitivity as a function of years in operation. The cyan (orange) band shows the sensitivity for rejecting the wrong ordering hypothesis for true normal (inverted) ordering, assuming fixed  $\sin^2 \theta_{13} = 0.022$ . The width of the bands covers the allowed values for  $\sin^2 \theta_{23}$  from 0.45 to 0.6. The black dot corresponds to the last reported SuperK neutrino mass ordering analysis [43]. For comparison, we also include the prediction of the next-generation long-baseline neutrino experiments that are supposed to start in mid-2027 in the case of HyperK and 2029 in the case of DUNE [44].

particular interest since measurements by current long-baseline experiments in the continental United States and Japan are in mild tension. This work shows, for the first time, that atmospheric experiments have the potential to weigh in on this tension. Finally, our work implies that before the operation of the next-generation neutrino detectors—DUNE, Hyper-Kamiokande, and IceCube-Gen2—we will have two independent measurements of the  $CP$  phase: one from the combination of accelerator neutrinos (i.e., T2K and NO $\nu$ A) and another one from the combination of atmospheric neutrinos.

The combination of the SuperK, IceCube Upgrade, ORCA, and HyperK has a twofold purpose of solving open questions in neutrino physics and providing initial input for the next generation of neutrino experiments. In this work, we develop for the first time the necessary tools to perform such a combined analysis along with the most realistic publicly available simulations for each experiment involved. All of this allows us to make the first in-depth analysis of those three experiments taking into account a detailed description and implementation of the detector responses and their common systematic uncertainties. The work performed here is well beyond what has currently been done in any prior global analysis of atmospheric neutrinos. The result is the realistic projection of the

sensitivity of atmospheric neutrinos to the remaining mixing parameters and the identification of the uncertainties limiting these measurements, thus establishing a competitive and independent approach from accelerators to the neutrino physics precision era.

The rest of this article is organized as follows. In Sec. II, we outline the primary characteristics of the atmospheric neutrino flux and discuss associated uncertainties. Section III delves into the interaction of these neutrinos with water, while Sec. IV focuses on key aspects of reconstructing these interactions. Atmospheric neutrinos need to cross Earth before reaching the detector, and the main aspect of the neutrino evolution is summarized in Sec. VI. In this analysis, we incorporate four experiments: Super-Kamiokande, IceCube Upgrade, ORCA and Hyper-Kamiokande. The scope of measurements conducted by each of these experiments are elucidated in Sec. VI. Section VII contains a description of the main results of this analysis, while Sec. VIII engages in a comprehensive discussion of their implications. We present our conclusion in Sec. IX.

## II. ATMOSPHERIC NEUTRINO FLUXES

In this section, we elucidate the key elements of the atmospheric neutrino flux that play a pivotal role in determining oscillation parameters. Additionally, we examine the primary sources of uncertainty influencing the measurement of this flux and propose a parametrization that incorporates them.

Atmospheric neutrinos are produced by the collision of cosmic rays with Earth's atmosphere. The primary spectrum of cosmic rays spans from MeV to EeV energies [48,49], and it is composed of free protons (approximately 80%) and bound nuclei (approximately 20%). Their interaction with nuclei in the atmosphere initiates hadronic showers on average about 20 km above the surface, producing copious amounts of mesons. Neutrinos are produced predominantly from the decay of muons, pions, and kaons, which dominate the muon-neutrino flux below 10, 100, and  $10^6$  GeV, respectively [50,51]. With  $\nu_\mu, \nu_e$  are also produced in the atmosphere, and above the TeV scale there also exists a  $\nu_\tau$  flux from the charmed mesons decays [52,53]. At the lowest energies, when decay of the mesons is prompt, the spectrum follows the cosmic-ray spectrum, but it softens by approximately one unit in spectral index as the mesons start interacting in the air [54]. In Fig. 4 (lower panel), we show the measurement of the total neutrino flux carried out by different experiments from approximately 100 MeV to approximately 100 GeV. We add the prediction from Honda *et al.* [55], which is used in this work as a benchmark scenario for the neutrino flux. We use the NUFLUX [56] package to interpolate those tables for the energy and directions relevant to this analysis. The three experiments considered in our analysis measure the flux at energies below approximately 100 GeV. The effective

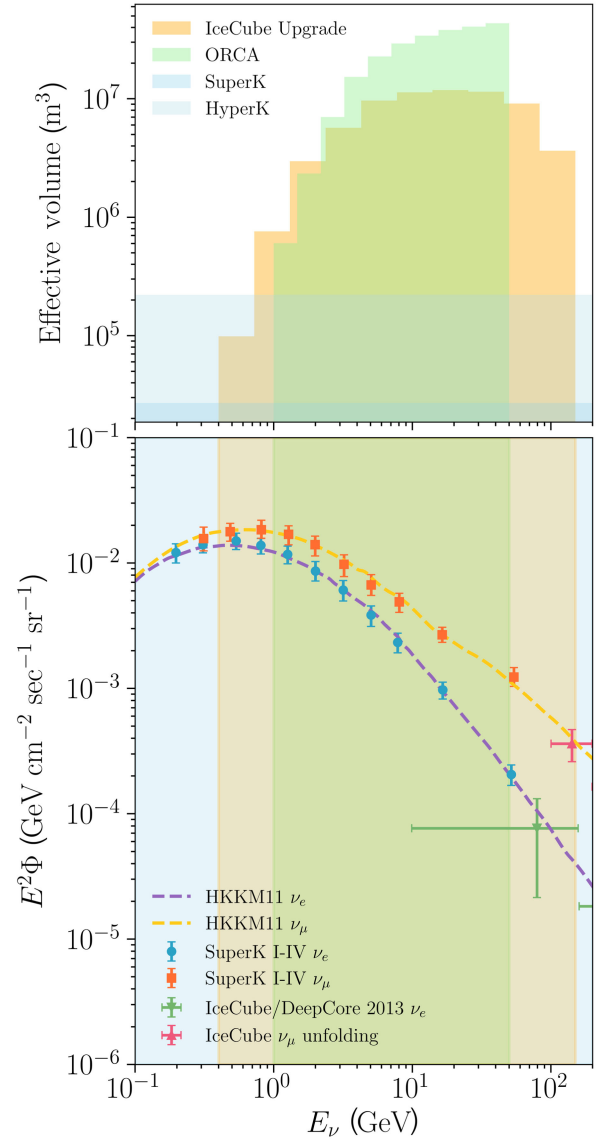


FIG. 4. Measurements of the atmospheric neutrino flux as a function of the energy. The total neutrino flux measured by different experiments [57–59] together with the energy range covered by the four experiments (SuperK, IceCube Upgrade, ORCA, and HyperK) considered in this analysis are shown in the lower panel. In the lower panel, we also include the flux prediction from the HKKM2014 model [55]. In the top panel, we have the effective volume for the three experiments as a function of the neutrino energy.

volume for SuperK, IceCube Upgrade, and ORCA as a function of the neutrino energy is shown in Fig. 4 (top panel).

The zenith distribution of the neutrino flux at the detector shows an enhancement for the horizontal directions due to the longer paths that mesons have to travel before hitting Earth. An example of this effect is shown in Fig. 5 (right) for  $\cos(\theta_{\text{zen}}) = 0$  for both flavor components of the flux at  $E = 10$  GeV, although the same effect also happens at larger energies. For energies where the mesons and muons

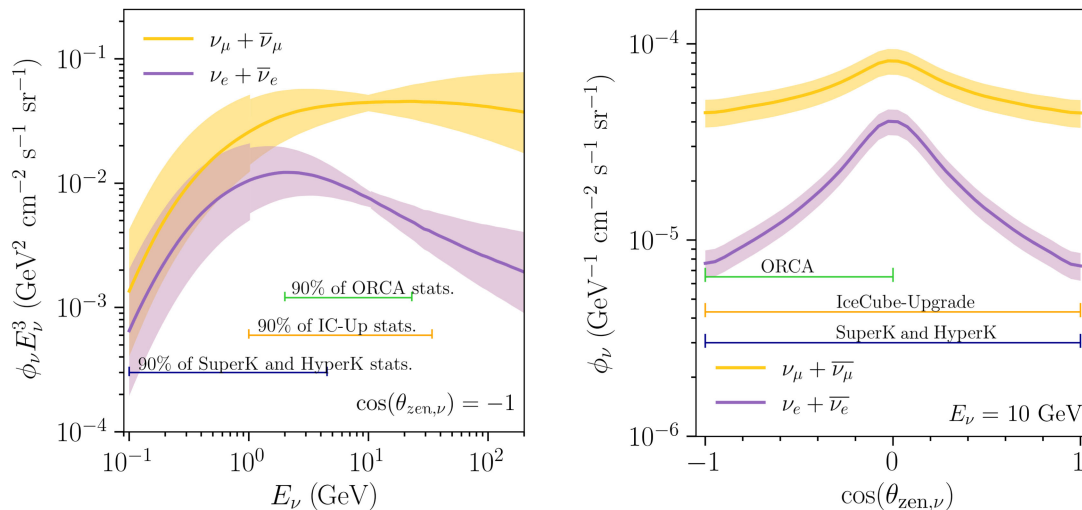


FIG. 5. Energy (left) and zenith (right) distribution of the atmospheric neutrino flux. The flux is based on the Honda *et al.* [55] calculation. Around the prediction for each flavor component of the flux at the detector, we show the  $1\sigma$  uncertainty band.

have decayed before reaching Earth, there is still a horizontal enhancement due to the spherical geometry [60] of the volume where the neutrinos are produced. The absorption of the mesons and muons by Earth also contributes to modifying the flavor composition of the initial flux. If all the parent particles are able to decay, we can expect that  $(\nu_e + \bar{\nu}_e)/(\nu_\mu + \bar{\nu}_\mu) \sim 1/2$ . As the energy increases and muons hit Earth, losing their energy, this ratio decreases in the meantime.

In the sub-GeV energy range, the flux shows additional anisotropies due to the interaction of the charged mesons with Earth's magnetic field. At low momentum, the mesons produced in the interaction of the cosmic rays get trapped by the magnetic field and can decay into neutrinos, enhancing the flux at lower energies. The trajectory of the primary cosmic rays that reach Earth also gets modified by the magnetic effects inducing an east-west asymmetry [61] and a dependence of the flux with the location of Earth [55]. Further, the interaction of the meson flux with Earth's magnetic field modifies the neutrino-to-antineutrino ratio. At lower energies, the multiple scatterings of the mesons wash out the differences between both fluxes. As the energy increases, the geomagnetic effect becomes less important on the meson fluxes, and the neutrino production is dominated by the primary flux mesons.

The uncertainties in the calculation of the atmospheric neutrino flux from cosmic-ray interactions described above arise from four factors: incident cosmic-ray flux, the hadronic interaction model, the atmospheric air density profile, and the magnetic effect at low energies. Precision measurements of Earth's atmospheric density have been performed by the NASA Atmospheric Infrared Sounder on board the Aqua satellite [62]. These data have been used to compute the atmospheric neutrino fluxes and study the effects of seasonal variations [63–65]. The effects of

seasonal variations on the atmospheric muon-neutrino flux are less than 10% for neutrinos below a TeV [64] and average out significantly for datasets that span multiple years. Additionally, cosmic-ray spectral measurements in the relevant energy range have been recently performed by AMS. Hadronic interaction models play a significant role in the uncertainty of atmospheric neutrino calculations; see Refs. [51,66] for reviews on this topic. The energy range relevant for our analyses is well covered by accelerator data predominantly by the NA49 and NA61 experiments at CERN, though measurements by HARP, PHENIX, and STAR are relevant on the lower- and higher-energy bands considered in this work [51,66]. These sources of uncertainty can be translated to bands on the atmospheric neutrino fluxes. As recently estimated [51], at below approximately 100 GeV, the normalization uncertainty of  $\nu_\mu + \bar{\nu}_\mu$  and  $\nu_e + \bar{\nu}_e$  is below 10%, while at energies below 10 GeV, the precision on the ratio of muon-to-electron neutrinos is known with an error below 2%. Additionally, at energies below approximately 10 GeV, the ratio of neutrinos to antineutrinos for muons is known with a precision between 1% and 5%, while for electrons this ratio is known to a precision of 10%.

To include all the uncertainties mentioned before, we use a similar parametrization of the flux as in Refs. [66,67]

$$\Phi_\alpha(E, \cos \zeta) = f_\alpha(E, \cos \zeta) \Phi_0 \left( \frac{E}{E_0} \right)^\delta \eta(\cos \zeta), \quad (1)$$

where  $f_\alpha(E, \cos \zeta)$  are the Honda table's values interpolated by NUFLUX [56]. The symbol  $\Phi_0$  describes the uncertainty over the normalization of the flux,  $(E/E_0)^\delta$  modifies the energy dependence of the flux, and  $\eta(\cos \zeta)_{u,d} = 1 - C_{u,d} \tanh(\cos \zeta)^2$  describes the relative uncertainty

TABLE I. Summary of atmospheric neutrino flux systematic uncertainties used in this work.

Systematic source	$1\sigma$ range
Normalization $E_\nu < 1$ GeV	25%
Normalization $E_\nu > 1$ GeV	15%
Spectral index	20%
Flux $\nu/\bar{\nu}$	2%
Flux $\nu_e/\nu_\mu$	2%
Up and horizontal	2%
Down and horizontal	2%

between horizontal and up-going or down-going directions. Table I summarizes the atmospheric flux systematic uncertainties of our analysis. For easy comparison, we use a systematic uncertainty budget that is consistent with recent SuperK [26] and IceCube [68] analyses. However, the choice of uncertainty parametrization used in this article is conservative given the discussion above, and is expected to be further improved by further measurements. In Fig. 5, we show the  $1\sigma$  range of the energy (left) and zenith (right) uncertainties used in our analysis.

### III. NEUTRINO-WATER CROSS SECTION

The experiments in this work share, in addition to the neutrino flux, the neutrinos' cross sections in water. These experiments cover a wide range of neutrino energies in which neutrinos may interact via the exchange of charged or neutral currents. The relevance of distinct interaction channels differs from one experiment to another, since they measure the atmospheric flux at distinct energy scales. Therefore, we need to study the different interaction channels as they may affect the determination of oscillation parameters in a different way in each experiment. In this section, we provide a concise overview of the essential aspects of the neutrino cross section that bear relevance to the determination of oscillation parameters.

Charged-current interactions produce a charged lepton that shares flavor with the original neutrino and are divided into three major contributions shown in Fig. 6.

- (i) Charged current quasielastic (CCQE): These interactions dominate in the lower-energy region, below 2 GeV, and scatter off one of the bound nucleons, exchanging a  $W^\pm$  boson, emitting the charged-lepton partner of the interacting neutrino. The outgoing nucleon is either a proton, for neutrinos, or a neutron, for antineutrinos. These interactions are most relevant in the sub-GeV region of the SuperK atmospheric neutrino dataset and the lowest-energy bins for IceCube Upgrade and ORCA, where the sensitivity to the  $CP$  phase resides. Additionally, this channel provides a clear link between the matter-antimatter character of the incoming neutrino and the presence of a neutron in the final state, which becomes relevant when introducing neutron-tagging capabilities in SuperK.

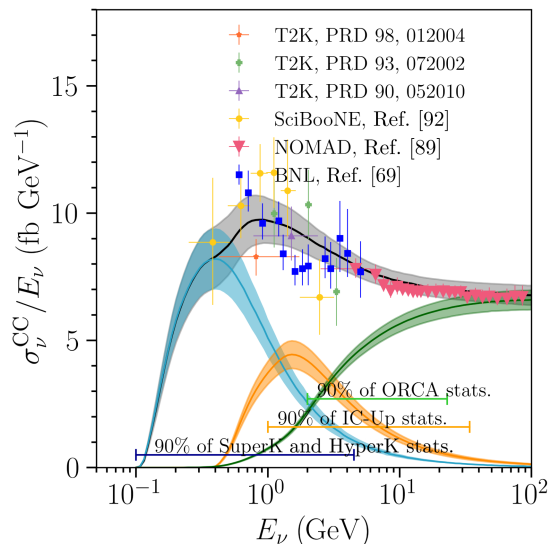


FIG. 6. Charged-current  $\nu_\mu$  cross section per nucleon as a function of the energy split by its main contributions, QE, RES, and DIS. The cross-section models used are from GENIE precomputed splines, shaded regions correspond to the  $1\sigma$  priors assumed in Table II, and data points correspond to the most relevant inclusive cross-section measurements for this work.

- (ii) Resonance production (CC RES): At slightly higher energies up to 4 GeV, neutrinos can excite an entire nucleon, producing a baryon resonance that, in turn, quickly decays into a nucleon and single or multiple mesons. The  $\Delta(1232)$  baryon resonance dominates this channel, producing a single pion in the final state. All three experiments are sensitive to this channel.

Similar to CCQE, in these interactions, antineutrinos tend to produce more neutrons than protons in the final state. Further, in single-pion production, neutrinos are linked to  $\pi^+$  and antineutrinos to  $\pi^-$ . In turn, oxygen atoms in water quickly absorb  $\pi^-$  before decaying, providing a potential signature to separate neutrinos from antineutrinos from the reconstruction of  $\pi^+$  decay products, namely, Michel electrons. The SuperK detector is sensitive enough to use these features, which in this energy region, provide sensitivity to the neutrino mass ordering from the core and mantle resonances between 2 and 10 GeV from the Mikheyev-Smirnov-Wolfenstein (MSW) effect of neutrinos propagating through Earth (Fig. 9).

Beyond resonance production, single-pion final states can also be produced from neutrinos coherently scattering the whole nucleus (Coh  $\pi$ ).

- (iii) Deep inelastic scattering (CC DIS): At energies above 4 GeV, neutrinos can scatter off a single quark inside the nucleon, producing the corresponding charged lepton plus a hadronic shower in the final state. In this type of event, the flavor reconstruction may get confused unless the outgoing charged lepton has sufficient momentum to be distinguished from the hadronic showers.

Given the large mass of the  $\tau$  lepton, this is the only channel allowed for charged-current tau neutrino interactions with a threshold of 3.5 GeV.

This channel dominates the neutrino interactions measured at IceCube Upgrade and ORCA, and thus the sensitivity to the neutrino mass ordering through the second Earth's matter-effect resonance and to the atmospheric squared-mass difference.

On the other hand, neutral-current interactions do not produce an accompanying charged lepton but a neutrino and, therefore, do not carry any information about the flavor of the incoming neutrino in water-Cherenkov detectors. Thus, these interactions are a background for the neutrino flavor oscillation analyses. For neutral currents, only analog resonance and deep-inelastic-scattering channels can be reconstructed in water-Cherenkov detectors if the produced mesons or hadronic showers are sufficiently energetic, or if the products decay to other detectable particles. An example of these interactions is the production of a  $\pi^0$  decaying to a pair of photons, which are a source of background for charged-current electronlike ( $e$ -like) events below 1 GeV in SuperK.

In addition, some products of primary interactions undergo secondary interactions within the nuclear media, making the final state of the neutrino interaction more complex and difficult to reconstruct and classify. Secondary interactions become more prominent at higher energies and obscure some distinct signatures expected from primary interactions, like the content of pions and neutrons, weakening the flavor identification as to the separation between neutrinos and antineutrinos in the case of SuperK.

Over the last four decades, several experiments have measured neutrino cross sections with different targets, and over a wide range of energies and channels relevant to this work. The first measurements were done in hydrogen and deuterium bubble chambers [69–71]. These experiments provided precise measurements but lacked the complexity and features of heavier target nuclei required in current and future neutrino oscillation experiments. The structure and kinematics of nucleons as well as the rescattering within the nucleus can potentially alter the neutrino interaction cross section and outcome, affecting the measurement of the oscillation parameters [72–74]. As neutrino physics developed, neutrino cross-section measurements on the relevant targets were necessary to account for these nuclear effects.

Both charged- and neutral-current neutrino interactions on water, carbon, and hydrocarbon targets are considerably well measured and theoretically understood [75–77]. Most of the existing measurements are for muon neutrinos and antineutrinos, and cover the previously sketched channels, ranging from 0.4 to  $\mathcal{O}(10^2)$  GeV and performed by Minerva [78–83], K2K [84–87], NOMAD [88–91], SciBooNE [92], and T2K [93–102]. Additionally, T2K has also performed measurements for sub-GeV electron neutrinos [103,104].

One of the remaining issues is to achieve the same precision for electron neutrinos and antineutrinos, for which the data are much scarcer since the beams are mainly made of muon neutrinos.

In addition to the aforementioned Minerva and T2K, there are other experiments with water targets in operation, such as ANNIE [105] and NINJA [106,107]. These experiments, together with near future detectors like Hyper-Kamiokande's Intermediate Water-Cherenkov Detector (IWCD) [28] and the upgrade of the current T2K's near detector ND280 [108], will play a crucial role in reducing the uncertainties of both muon- and electron-neutrino and antineutrino cross sections as well as differential cross sections at energies from hundreds of MeV to a few GeV on a water target. Additionally, the upgrade of ND280 will measure the ratio between carbon and oxygen to better precision, enabling a more precise extrapolation of cross-section measurements on carbon and hydrocarbon targets. Moreover, the tagging of neutrons from neutrino interactions is proven to be an effective tool for separating neutrinos from antineutrinos. It is expected that the ANNIE and IWCD experiments will be Gd-doped detectors exposed to high-intensity neutrino beams, thus providing valuable input to reduce the current neutron production uncertainties.

In addition to more experimental measurements, the development of more precise nuclear and interaction models is crucial. In this context, two topics will be of great importance in the coming years for neutrino physics: first, the model-independent reassessment of bubble chamber data and, second, the deeper study of nucleon form factors and resonance production from updated models and lattice QCD calculations [109–111]. The latter work would be especially relevant for the CCQE and RES channels.

For the charged-current tau neutrino, data are much more limited; they come primarily from the DONuT [112] and OPERA experiments [113] and, more recently, from tau appearance measurements in the atmospheric neutrino flux from IceCube and SuperK [114,115]. These measurements found the cross section to be in good agreement with the expectations within 10% of the expected value. Tau appearance does not play a significant role in extracting the parameters of interest in this article, and thus we do not discuss them further.

For a detailed review of neutrino cross sections and available data, the reader is referred to Refs. [44,116–121].

The systematic uncertainties assumed in this work are summarized in Table II and follow the ranges assumed by the official oscillation analyses from each of the experiments considered in this work. During the upcoming data-taking period of IceCube Upgrade, ORCA, and SuperK, it is expected that the neutrino cross-section uncertainties will further improve with new data from experiments in operation and theoretical development. These measurements and theoretical developments are motivated by the

TABLE II. Summary of the neutrino-water interactions systematic uncertainties used in this work.

Systematic source	$1\sigma$ range
CCQE	10%
CCQE $\nu/\bar{\nu}$	10%
CCQE $e/\mu$	10%
CC1 $\pi$ production	10%
CC1 $\pi$ $\pi^0/\pi^\pm$	40%
CC1 $\pi$ $\nu_e/\bar{\nu}_e$	10%
CC1 $\pi$ $\nu_\mu/\bar{\nu}_\mu$	10%
Coh. $\pi$ production	100%
Axial mass ( $M_A$ )	10%
CC DIS	5%
NC hadron prod.	10%
NC over CC	20%
$\nu_\tau$	25%
Neutron production (SuperK only) [122]	15%

upcoming next-generation neutrino detectors DUNE and Hyper-Kamiokande.

#### IV. PHYSICS OF WATER-CHERENKOV DETECTORS

Because of their large active and instrumented volumes, water- or ice-Cherenkov detectors have proven to be very effective and successful technology for measuring the properties of neutrinos.

In these kinds of detectors, neutrinos interact with the nuclei in water molecules producing several particles depending on the primary interaction channel and subsequent secondary interactions within the nuclear media. Charged particles with momenta above a given threshold determined by the refractive index of the medium emit Cherenkov radiation detected with photomultiplier tubes (PMTs). Ice and water have slightly different refractive indexes [124], and thus, Cherenkov energy thresholds; namely, 0.13 and 1.2 GeV in Antarctic ice and 0.16 and 1.4 GeV in water for muons and protons, respectively.

Furthermore, both media exhibit well-understood light-propagating properties enabling reliable event reconstruction. This is clearly shown by all three experiments considered in this work. On the one hand, thanks to its large photocoverage and the exhaustive control of the water conditions, SuperK can reconstruct very low-energy events (MeV scale), which gives a comprehensive reconstruction of atmospheric neutrino events at energies below 1 GeV. On the other hand, the IceCube Upgrade and ORCA experiments are capable of precisely parametrizing the optical properties of Antarctic ice and Mediterranean seawater, so it is possible to control such large volumes of unprocessed media and use them as particle physics detectors with energies as small as 1 GeV. In this context, the ORCA experiment provides a better directional reconstruction than IceCube where there is

more scattering of photons due to the presence of air bubbles trapped in the ice. As charged particles propagate through a medium, they polarize the medium around them. When these particles move faster than light in that medium, photons from the polarization, unable to keep up with the particles' pace, form a characteristic cone of light around the direction of motion, with a characteristic opening angle depending on the medium's refractive index. The detection of this radiation allows the reconstruction of the direction and production vertex of the charged particle. Additionally, being proportional to the number of photons emitted, the momentum of the particle is inferred from the charge collected by the PMTs.

In the context of neutrinos, this means water-Cherenkov (WC) detectors can reliably reconstruct the promptly charged leptons that originate from a neutrino charged-current interaction, namely,  $e^\pm$  and  $\mu^\pm$  from electron and muon (anti)neutrinos, respectively. Moreover, in large-photo-coverage experiments, some particles are identified based on the ring patterns; electrons produce diffuse ring patterns due to the electromagnetic showers produced as they propagate through water ( $e$ -like or showers), whereas muons, being more massive, produce rings with sharper edges ( $\mu$ -like or tracks). Other particles such as high-energy photons and charged pions can be detected and reconstructed similarly, the former with a pattern practically indistinguishable from showers and the latter from tracks. All these features extend the capabilities of neutrino WC detectors, allowing for a complete reconstruction of the particles in the final state of the neutrino interaction as well as the decay products from heavier short-lived particles and other charged particles produced in secondary interactions.

There are, however, differences in the reconstruction among the detectors considered. In the case of SuperK, the Cherenkov cone gets projected to the densely instrumented inner surface, which registers all the signals produced in the event. In the case of IceCube and ORCA, strings of PMTs are scattered throughout the volume, enabling the measurement of the energy loss of particles as they travel through the ice (IceCube) and seawater (ORCA) at each step of the track. See Refs. [125–127] for recent discussions on reconstruction on these type of detectors.

An additional yet relevant point is the detection of neutrons in WC detectors. Currently, in the context of atmospheric neutrinos, this applies only to SuperK. Despite having a null electric charge, neutrons get captured by hydrogen atoms of water, forming an excited state of deuterium. Its deexcitation emits a 2.2-MeV photon, which is detected with an efficiency of approximately 20%. Despite the modest tagging efficiency, this capability adds more information to the reconstructed final state of the interaction, improving the oscillation analysis sensitivity, which we discuss in Sec. VIB.

Additionally, given the proven relevance of neutron tagging [128], SuperK is being upgraded to dissolve a

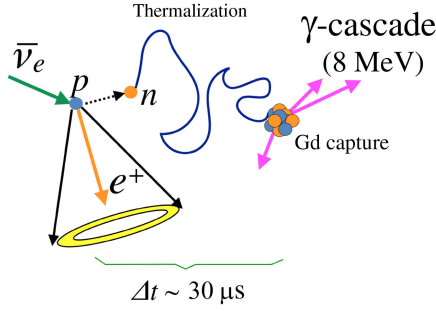


FIG. 7. Diagram showing neutron tagging on gadolinium in an inverse- $\beta$  interaction.

gadolinium (Gd) salt in the water to improve the detection of neutrons through their capture on this element [129]. Gadolinium is the stable isotope with the largest thermal neutron absorption cross section, which, together with the emission of an 8-MeV cascade of photons, as shown in Fig. 7, enhances the neutron detection efficiency up to approximately 80%.

## V. NEUTRINO OSCILLATIONS

In the  $3\nu$  scenario, neutrino evolution is described by six parameters: two mass-squared differences ( $\Delta m_{31}^2$  and  $\Delta m_{21}^2$ ), three mixing angles ( $\theta_{12}$ ,  $\theta_{13}$ , and  $\theta_{23}$ ), and a complex phase that parametrizes the violation of the  $CP$  symmetry in the lepton sector. The so-called solar parameters ( $\Delta m_{21}^2$  and  $\theta_{12}$ ) have been measured by solar experiments and KamLAND [130–133] looking for the disappearance of the electron neutrinos or antineutrinos. Reactor experiments with a baseline of  $\mathcal{O}(10^0 \text{ km})$  and using a configuration with a near and a far detector has determined  $\theta_{13}$ , becoming the most precisely measured parameter to date [134–136]. Finally, the atmospheric parameters ( $\Delta m_{31}^2$  and  $\theta_{23}$ ) and the  $CP$ -violation phase require high-energy beams, and therefore are constrained by long-baseline experiments [24,137–140]. Using a  $\nu_\mu$  flux with energies at or near the GeV scale, those experiments search for the disappearance of muon neutrinos ( $\nu_\mu \rightarrow \nu_\mu$ ) and for the appearance of electron neutrinos ( $\nu_\mu \rightarrow \nu_e$ ). In the case of the muon-disappearance channel, since the matter effects are suppressed by  $\sin^4 \theta_{23}$  [141], the oscillation probability at leading order [142] can be written as

$$P_{\mu\mu} \approx 1 - 4|U_{\mu 3}|^2(1 - |U_{\mu 3}|^2) \sin^2 \Delta m_{\mu\mu}^2, \quad (2)$$

where

$$\Delta m_{\mu\mu}^2 = \sin^2 \theta_{12} \Delta m_{31}^2 + \cos^2 \theta_{12} \Delta m_{32}^2 + \cos \delta_{CP} \sin \theta_{13} \sin 2\theta_{12} \tan \theta_{23} \Delta m_{21}^2, \quad (3)$$

showing that we can constrain  $\Delta m_{\mu\mu}^2$  and  $\sin^2 2\theta_{23}$  by looking at the muon distribution in the detector.

In the appearance channel, the matter effects are more important. To describe long-baseline experiment (LBL) sensitivity using this channel, we use an expression valid in a constant matter neutrino evolution [143–145] given by

$$P_{\mu e} \approx 4 \sin^2 \theta_{13} \sin^2 \theta_{23} \frac{\sin^2 \Delta_{31}(1 - asA)}{(1 - asA)^2} + s \frac{\Delta m_{21}^2}{|\Delta m_{31}^2|} \sin 2\theta_{13} \sin 2\theta_{12} \sin 2\theta_{23} \times \cos(s\Delta_{31} + a\delta_{CP}) \frac{\sin \Delta_{31} A \sin \Delta(1 - asA)}{A(1 - asA)}, \quad (4)$$

where  $a = 1$  for neutrinos and  $a = -1$  for antineutrinos,  $s = \text{sign}(\Delta m_{31}^2)$ , and  $\Delta_{ij} = \Delta m_{ij}^2 L / 4E$ . The matter effects in this channel are introduced via the term  $A = 2EV / \Delta m_{31}^2$ , where  $V$  is the matter potential. The dependence of this channel on the mass ordering is proportional to the matter effects. The  $\nu_e$  appearance also depends on  $\sin^2 \theta_{23}$  bringing the possibility to resolve between both  $\theta_{23}$  octants. Also, as we see from Eq. (4), using this channel we have a dependence on  $\theta_{13}$ . Moreover, the possibility of long-baseline experiments in running in neutrino and antineutrino modes (or in the atmospheric case, having a mixed beam of neutrinos and antineutrinos) enables these experiments to resolve the differences in the oscillation of both modes. The comparison of the neutrino and antineutrino oscillation patterns can be translated into a measurement of  $\delta_{CP}$ .

The latest results of the global analyses indicate that some of those parameters can be constrained to the percent level [9,146,147], although there are still several sizeable uncertainties in the  $3\nu$  mixing scenario. Among the less-constrained parameters, we have  $\theta_{23}$ , for which values above and below maximal mixing are allowed within  $1\sigma$ ; for the mass ordering, we have a  $2\sigma$  preference for NO [148], and  $\delta_{CP}$ , for which just a small region around  $\pi/2$  is excluded by T2K and SuperK at  $3\sigma$  CL. Atmospheric neutrinos can contribute to narrowing down those uncertainties.

### A. Neutrino evolution through Earth

The large range of baselines covered by atmospheric neutrinos that extend from  $\mathcal{O}(10 \text{ km})$  to  $\mathcal{O}(10^4 \text{ km})$ , and the vast energy range where the flux can be measured from  $\mathcal{O}(10^{-2} \text{ GeV})$  to  $\mathcal{O}(10^5 \text{ GeV})$  ensures the access to a vast neutrino oscillation phenomenology, as we can see in Figs. 8 and 9.

In the sub-GeV region, and for baselines of approximately 1000 km, the neutrino evolution is dominated by  $\Delta m_{21}^2$ . The finite-energy resolution makes the experiments inaccessible to the oscillation driven by  $\Delta m_{31}^2$  and  $\Delta m_{32}^2$ .

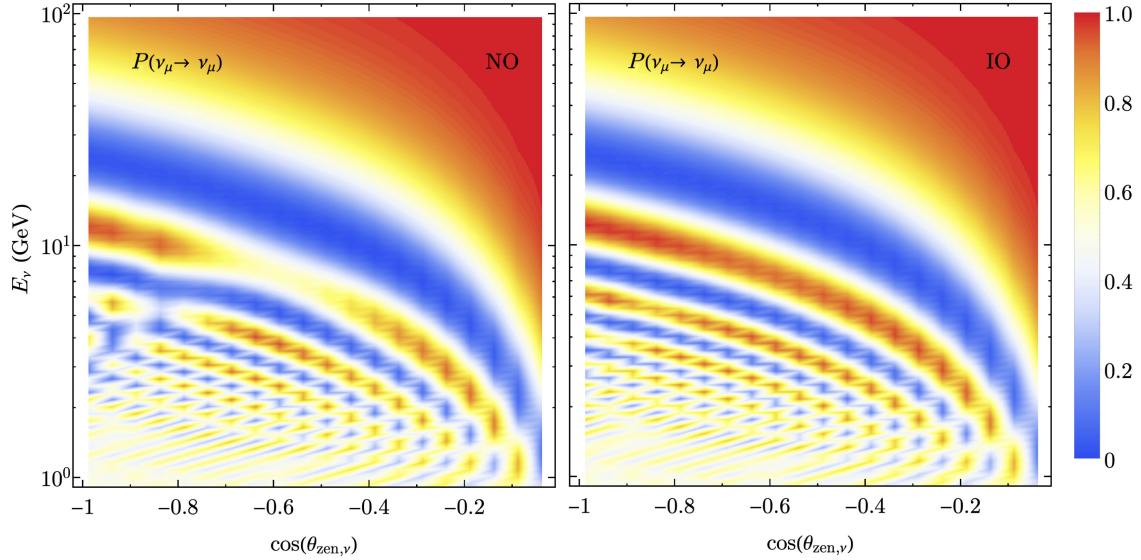


FIG. 8. Muon-disappearance probability. For energies above 1 GeV and all the trajectories crossing Earth [ $-1 < \cos(\theta_{\text{zen}}) < 0$ ], we compute  $P(\nu_\mu \rightarrow \nu_\mu)$  for normal (left) and inverted (right) mass ordering. We consider the PREM for Earth matter distribution.

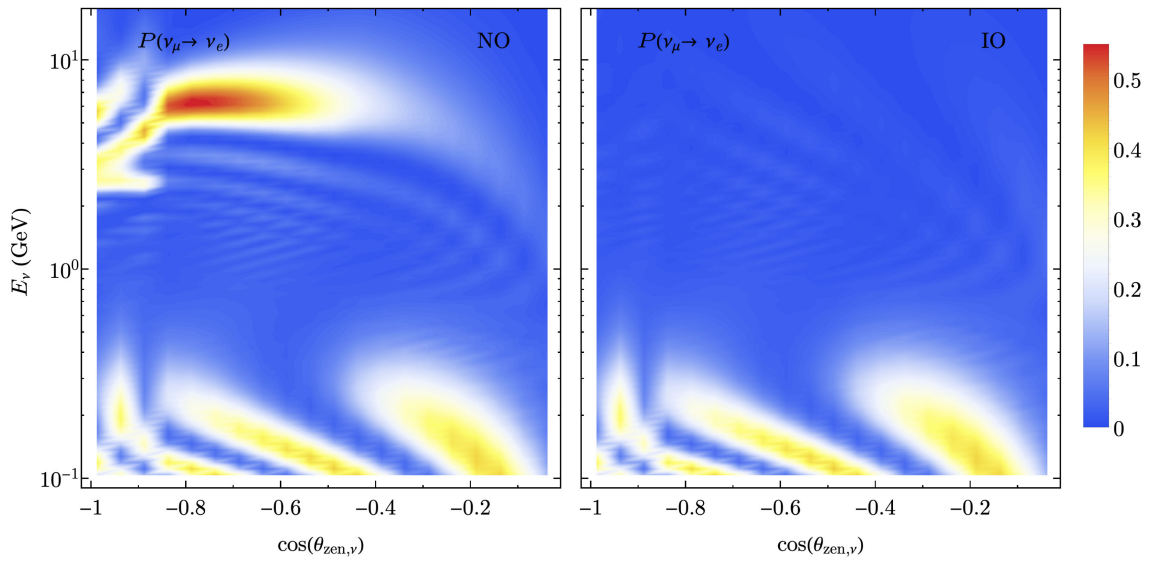


FIG. 9. Electron-appearance probability. Similar to Fig. 8, we compute  $P(\nu_\mu \rightarrow \nu_e)$  for both mass orderings, normal (left) and inverted (right). In this case, we consider neutrinos with energies between 0.1 and 15 GeV.

The average over those two oscillatory terms enhances the effects of  $\delta_{CP}$  over neutrino evolution [149,150]. The asymmetry between neutrino and antineutrino oscillation comes through the Jarlskog invariant [151,152] defined as  $J = \Im[U_{ai}U_{aj}^*U_{\beta i}^*U_{\beta j}] = J_r \sin \delta_{CP}$ , where we factorize the dependence with  $\delta_{CP}$ . In vacuum, the  $CP$ -violation term is given by the product of the three oscillation wavelengths [153] and the Jarlskog invariant, namely,

$$P_{CP} = -8J_r \sin \delta_{CP} \sin \Delta_{21} \sin \Delta_{31} \sin \Delta_{32}, \quad (5)$$

where  $\Delta_{ij} = \delta m_{ij}^2 L / 4E$ . The average over the two largest mass splittings suppresses the  $P_{CP}$  term by approximately 1/2 [154]. Fig. 10 shows the electron- and muon-appearance probability for two values of  $\delta_{CP} = 0$  and  $\pi$ . In the case of  $CP$  conservation, both probabilities are the same, as seen in the top and bottom panels of the figure. As  $\delta_{CP}$  takes a different value, both appearance channels separate, increasing the sensitivity over that parameter [155]. The  $CP$  violation results in a different normalization of the probability and a shift in the oscillation phase: these effects are quite broad in energy and more relevant specifically in the

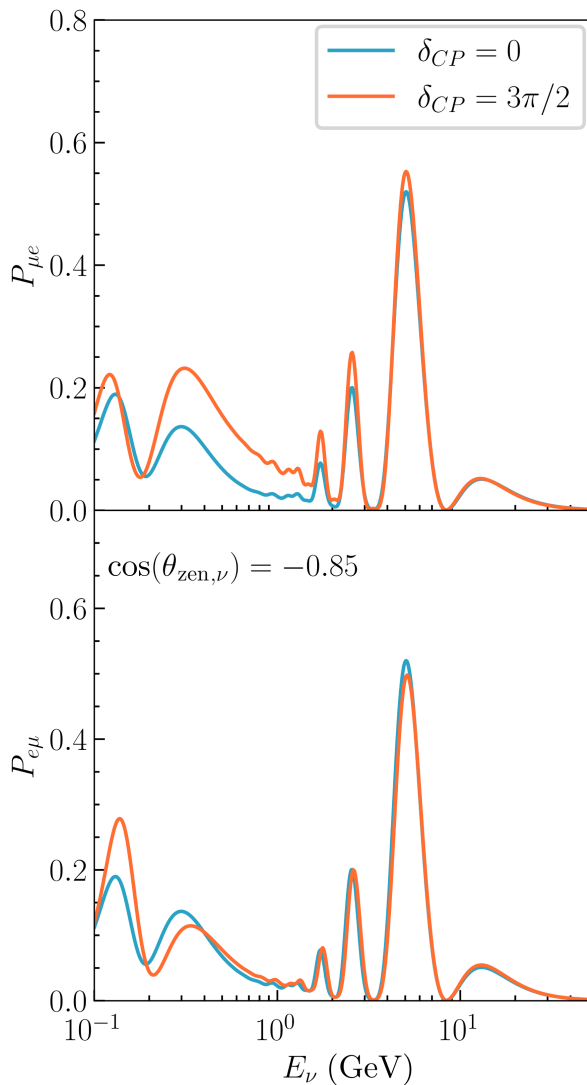


FIG. 10. Electron- (top) and muon- (bottom) appearance probabilities for  $\cos(\theta_{\text{zen}}) = -0.85$ . We show the impact of  $\delta_{CP}$  in both oscillation channels. The fast oscillations are smeared assuming a Gaussian uncertainty of  $5\% E/\text{GeV}$ .

sub-GeV energy range. The matter effects depend on the neutrino trajectory along Earth and create a dependence on the  $CP$  effects with the neutrino direction.

As the neutrino energy rises, the matter effects become more important. At the GeV energy scale and for trajectories crossing the mantle, there is an enhancement of the effective mixing angle  $\tilde{\theta}_{13}$  due to the coherent-forward elastic scattering of the neutrinos with the electrons in Earth, the so-called MSW effect [7,156]. The matter-modified mixing angle is given by

$$\sin 2\tilde{\theta}_{13} = \frac{\sin 2\theta_{13}}{\sqrt{(\cos \theta_{13} - 2EV/\Delta m_{31}^2)^2 + \sin^2 2\theta_{13}}}. \quad (6)$$

For energies around 6 GeV and densities around  $5 \text{ g/cm}^3$ ,  $\sin 2\tilde{\theta}_{13}$  becomes maximal, giving rise to an enhancement

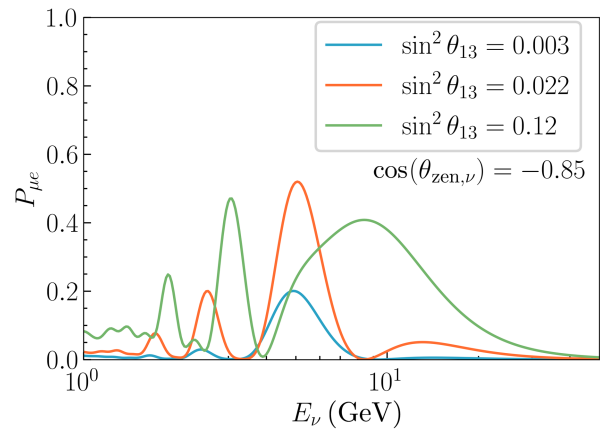


FIG. 11. Electron-appearance probability for different values of  $\sin^2 \theta_{13}$ . The neutrino direction is fixed to  $\cos(\theta_{\text{zen}}) = -0.85$ . The fast oscillations that happen for  $E \sim \text{GeV}$  are smeared assuming a Gaussian uncertainty of  $5\% E/\text{GeV}$ .

of the flavor conversion; see in Fig. 11. The location of the resonance is controlled by  $\sin^2 \theta_{13}$  for a given value of  $\Delta m_{31}^2$ , providing sensitivity to this angle. As  $\sin^2 \theta_{13}$  becomes larger, the resonance moves to lower energies and densities. The opposite happens if  $\sin^2 \theta_{13}$  becomes smaller, and we need larger energies and densities to meet the resonant condition. For very small values of  $\sin^2 \theta_{13}$ , the oscillation length at the resonance becomes larger than the size of Earth [141], making it impossible to get a large flavor conversion with atmospheric neutrinos, as is the case with the blue line in Fig. 11.

Beyond the MSW effect, at energies around 1 GeV, the oscillation is enhanced for some trajectories crossing Earth's core and mantle due to the matter distribution, the so-called parametric resonance [67,157–168]. Both types of resonances happen for neutrinos if the mass ordering is normal and for antineutrinos in the case of inverted ordering, as shown in Figs. 8 and 9. The differences in the flux and the cross section for both fermions bring the possibility to measure the neutrino mass ordering using atmospheric neutrinos.

In the multi-GeV scale, the neutrino oscillation length gets longer, and the neutrino oscillation is dominated by  $\Delta m_{31}^2$  and  $\theta_{23}$ . The first oscillation minimum for  $P(\nu_\mu \rightarrow \nu_\mu)$  happens at  $E \sim 20 \text{ GeV}$  for baselines that cross Earth; see Fig. 8. The energies where that oscillation minimum happens depend on  $|\Delta m_{31}^2|$ , and the oscillation amplitude is controlled by  $\sin^2 2\theta_{23}$ , as shown in Fig. 12 [169]. It is important to notice that the octant of  $\theta_{23}$  can be measured with atmospheric neutrinos in two ways as shown in Fig. 12: similar to LBL experiments through the electron-appearance channel as it is proportional to  $\sin^2 \theta_{23}$ , Equation (4), and through muon disappearance as matter effects break its dependence with  $\sin 2\theta_{23}$  due to the enhancement of  $\sin 2\tilde{\theta}_{13}$ .

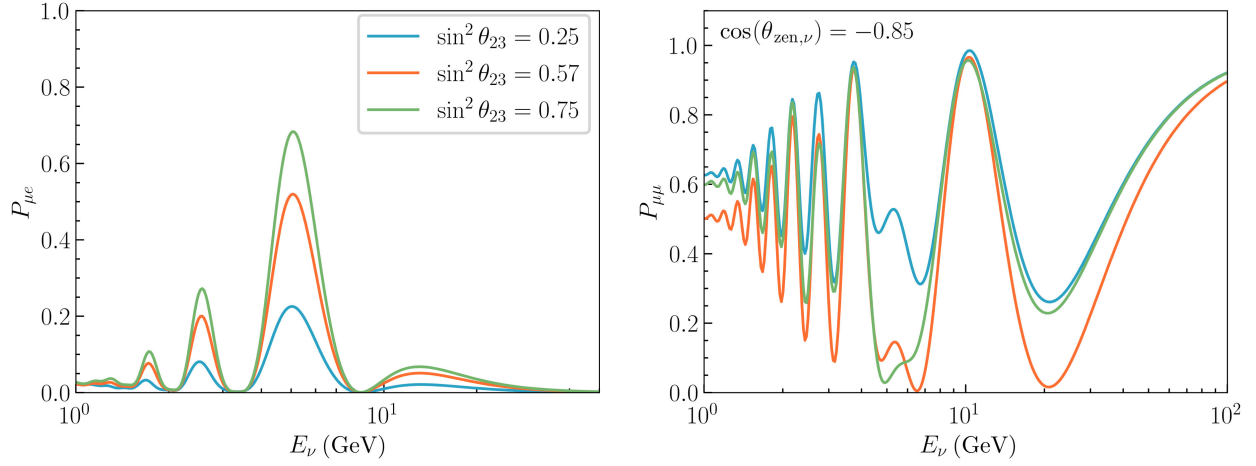


FIG. 12. Electron-appearance (left) and muon-disappearance (right) probabilities for  $\cos(\theta_{\text{zen}}) = -0.85$ . We show the impact of  $\sin^2 \theta_{13}$  in both oscillation channels. The fast oscillations are smeared assuming a Gaussian uncertainty of 5%  $E/\text{GeV}$ .

In this analysis, we numerically solve the neutrino evolution using NUSQUIDS [170]. For Earth matter density, we used the preliminary reference Earth model [171] (PREM), which divides Earth into 11 concentric layers, and for each of the layers, the density is given by a polynomial function that depends on its distance to the center of Earth. As a benchmark scenario for the mixing parameters, we follow the NU-FIT results [146]. For the solar parameters, we use  $\Delta m_{21}^2 = 7.42 \times 10^{-5} \text{ eV}^2$  and  $\sin^2 \theta_{12} = 0.304$  that are fixed in the whole analysis. The reactor angle is fixed at  $\sin^2 \theta_{13} = 0.022$  unless otherwise specified. For the atmospheric parameters, we assume  $\Delta m_{31}^2 = 2.5 \times 10^{-3} \text{ eV}^2$  and  $\sin^2 \theta_{23} = 0.572$ , and for the  $CP$ -violation phase  $\delta_{CP} = 234^\circ$ . This is summarized in Table III.

## VI. EXPERIMENTAL ANALYSES

To analyze the sensitivity to the neutrino oscillation parameters, we produce an Asimov dataset for each experiment, and perform a combined fit to the Monte Carlo simulation assuming different values of the oscillation parameters sampled from two four-dimensional ( $\Delta m_{31}^2$ ,

TABLE III. Summary of the true values assumed for three-flavor neutrino oscillation parameters and their treatment in the oscillation analysis.

Parameter	True value	Constraints
$\sin^2 \theta_{12}$	0.304	Fixed
$\sin^2 \theta_{13}$	0.022	Free
$\sin^2 \theta_{23}$	0.572	Free
$\delta_{CP}$	4.082	Free
$\Delta m_{21}^2$ (eV <sup>2</sup> )	$7.42 \times 10^{-5}$	Fixed
$\Delta m_{31}^2$ (eV <sup>2</sup> )	$2.50 \times 10^{-3}$	Free
Ordering	Normal	Free

$\theta_{23}$ ,  $\theta_{13}$ , and  $\delta_{CP}$ ) grid of points, one for each neutrino ordering. To reduce the impact of stochastic uncertainties from the simulations, we produce large-exposure Monte Carlo datasets for each experiment.

We bin the events in observable quantities, which differ from experiment to experiment and are discussed in the following subsection. We then construct the following test statistic,  $\chi^2$ , to compare the data with prediction. This is given by Eq. (7),

$$\chi^2 = 2 \sum_{\text{expt}} \sum_{i \in \text{bins}} \left[ \mu_i \left( 1 + \sum_{j \in \text{syst}} \eta_j f_{ij} \right) - O_i \right. \\ \left. + O_i \times \log \left( \frac{O_i}{\mu_i (1 + \sum_{j \in \text{syst}} \eta_j f_{ij})} \right) \right] \\ + \sum_{j \in \text{syst}} \left( \frac{\tilde{\eta}_j - \eta_j}{\sigma_j} \right)^2, \quad (7)$$

where  $\mu_i$  and  $O_i$  are the expected number of events in the  $i$ th bin, respectively, and  $f_{ij}$  is the fractional change in the number of events in the  $i$ th bin due to the  $j$ th systematic source of uncertainty which takes value  $\eta_j$  and has  $\tilde{\eta}_j$  nominal value with  $\sigma_j$  error size.

The first term in Eq. (7) is the negative times two of the log-likelihood ratios between the Asimov dataset and the MC at a given point in the oscillation parameter space assuming Poisson statistics, and the last term takes into account the penalty from each source of systematic uncertainty for which Gaussianity is assumed. The Asimov dataset is fitted against the MC using a binned  $\chi^2$  method assuming the number of events per bin follows a Poisson statistic. For introducing the effect of systematic uncertainties, the number of entries in each bin is reweighted accordingly, and an additional penalty term is introduced in Eq. (7); see Ref. [172] for details.

Minimizing Eq. (7) requires us to solve the system of equations defined by  $\nabla\chi^2 = \vec{0}$  over all systematic uncertainties. This procedure brings the Asimov dataset and MC into the best agreement allowed by the size of systematic uncertainties. Usually, this process requires extensive CPU resources as it relies on the numerical computation of partial derivatives with respect to all systematic sources, which has to be repeated for all points in the defined grid of oscillation parameters to be tested while managing large simulation files. This problem can be alleviated by analytically computing the Jacobian of Eq. (7), at the cost of implementing in the code the partial derivatives of the expected number of events in each bin for each systematic source, as shown in Eq. (8). Such an implementation improves the convergence time to a minimum by almost 2 orders of magnitude in this analysis and provides more robust minimization. For the minimization of  $\chi^2$  we use the SCIPY PYTHON package [173]

$$\nabla_j\chi^2 = 2\sum_{\text{expt}} \sum_{i \in \text{bins}} \left[ \left(1 - \frac{O_i}{\mu'_i}\right) \frac{\partial\mu'_i}{\partial\eta_j} \right] + 2\left(\frac{\tilde{\eta}_j - \eta_j}{\sigma_j^2}\right),$$

where  $\frac{\partial\mu'_i}{\partial\eta_j} = \mu_i f_{ij}$ . (8)

The events are divided into the samples according to the definitions of each experiment and binned by their reconstructed zenith angle and energy as explained in Secs. VI A, VI B, VI D, and VI E.

The  $f_{ij}$  are introduced by computing them on run-time before the fit on an event-by-event basis or readout from publicly available tables. Unlike prior global analyses of atmospheric neutrinos, flux and cross-section systematics are common to all experiments considered, while detector systematics are applied only to each experiment.

As mentioned earlier, in this work, we consider four experiments: SuperK, IceCube Upgrade, ORCA, and HyperK. Additionally, we consider the three distinct phases of operation within SuperK: SuperK without H-neutron tagging (SuperK), SuperK with H-neutron tagging (SK-Htag), and SuperK with SKGd. The phases of SuperK are treated in the analysis as three independent data-taking experiments, with uncorrelated detector systematics. The first phase of SuperK covers the first three runs of the experiment, from SuperK-I to SuperK-III; SK-Htag covers the detector from SuperK-IV to SuperK-V with neutron-tagging capabilities on hydrogen; finally, SKGd covers the projected running time of SuperK with gadolinium enabling improved neutron tagging. In terms of exposure, we assume the full data-taking periods through SuperK-I to SuperK-V as reported in Ref. [43]. For SKGd, we project five years of operation with the final concentration of Gd dissolved in water, 0.2%, starting in 2025.

For the soon-to-be-deployed IceCube Upgrade and ORCA, we conservatively foresee five and three years of

operation starting in 2025 and 2027, respectively. For HyperK, we assume 2.5 years of operation starting in mid-2027 as foreseen by the collaboration. Thus, the combined analysis in the report assumes the running of SuperK until the last reported exposure time, the SKGd and IceCube Upgrade data-taking period extending from 2025 until 2030, and ORCA from 2027 to 2030. Additionally, HyperK is projected to be completed by mid-2027, ensuring a large amount of statistics by 2030, and thus, it is included in the fit. The situation is less certain for DUNE, as its final volume has not been defined; for this reason, it is not included in the fit. Nonetheless, its expected performance is described in Sec. VI F. According to the status of construction, this fit conservatively considers the neutrino oscillation measurement picture these experiments will provide by the end of the decade.

The combined fit is then performed over a total of 3595 bins (SuperK-I to SuperK-III, 459; SuperK-IV to SuperK-V, 539; SKGd, 539; IceCube Upgrade, 800; ORCA, 180; HyperK, 1078) from events classified in 75 samples (SuperK-I to SuperK-III, 16; SuperK-IV to SuperK-V, 18; SKGd, 18; IceCube Upgrade, 2; ORCA, 3; HyperK, 18). A total of 103 systematic uncertainties are considered, 20 of which come from flux and cross section and are common to all experiments, and the rest are related to each detector (SuperK-I to SuperK-III, 16; SuperK-IV to SuperK-V, 17; SKGd, 17; IceCube Upgrade, 6; ORCA, 10; HyperK, 17).

### A. Super-Kamiokande

SuperK is a 50-kton cylindrical water-Cherenkov detector located in Kamioka, Japan. The detector is instrumented with more than 11 000 20-in. PMTs in the inner surface and facing inwards the fiducial volume. The mountain above shields the experiment from most of the cosmic-ray muons and the large photocoverage enables the measurement of low-energy atmospheric neutrinos up to 100 MeV [174].

SuperK started its operation in 1996 and has largely contributed to the current knowledge of neutrinos; particularly, it contributed to the discovery that neutrinos have a definite mass by measuring oscillations in atmospheric neutrinos [175]. Over the years, the experiment went through various phases, from SuperK-I to the current SuperK-VI [43]. Since 2020, the experiment has been undergoing a major upgrade going from an ultrapure to a Gd-doped water-Cherenkov detector [176], which will improve its capabilities by enabling highly efficient neutron tagging on gadolinium.

After more than 25 years of nearly continuous operation, SuperK data provide a very comprehensive picture of neutrino oscillations measuring solar [131,177,178], accelerator—serving as K2K's [179–181] and T2K's [46,182–185] far detector—and atmospheric fluxes [59,115,186–189]. From the latter and according to Ref. [47], SuperK has been able to constrain the values of the atmospheric parameters

$\Delta m_{31}^2 = 2.50_{-0.20}^{+0.13} \times 10^{-3} \text{ eV}^2$  and  $\sin^2 \theta_{23} = 0.588_{-0.064}^{+0.031}$ , and of the  $CP$  phase  $\delta_{CP} = 4.18_{-1.61}^{+1.41}$ , assuming  $\theta_{13}$  is constrained by reactor experiments. The results also show a preference for normal ordering at approximately  $2\sigma$  level.

Recently, due to the knowledge of the detector, the SuperK Collaboration was able to extend the fiducial volume by 20%, from the usual 22.5 to 27 kton in all running periods [43], enlarging the sample size and thus its sensitivity. We assume this improved fiducial volume in our analysis.

For this work, we develop a detailed Monte Carlo simulation to predict the atmospheric neutrino event rate at SuperK. First, neutrino events interacting with a water target are generated using the GENIE event generator [190]. Then, we implement software emulating the SuperK reconstruction procedures, efficiencies, and resolutions based on publicly available information. In the end, we produce a simulation equivalent to 300 years for each phase of the experiment following the event categories defined in each case.

The official atmospheric neutrino analysis from SuperK separates events into three categories depending on their morphology: fully contained (FC), partially contained (PC), and upward-going muons (Up- $\mu$ ). In this work, we simulate only the first two, as the latter has very mild impact on the sensitivity and is statistically dominated by IceCube Upgrade and ORCA.

The reconstruction is focused on the FC events as they carry the most information and are the most abundant in the energy region sensitive to the oscillation parameters, from 0.1 to 20 GeV. Fully contained events get categorized into single ring or multiring depending on the number of rings,

sub-GeV or multi-GeV attending to their reconstructed visible energy, and  $e$ -like or  $\mu$ -like in terms of the reconstructed ID of the most energetic ring. In addition, depending on other reconstructed variables, events get further divided to distinguish neutrinos from antineutrinos, and charged-current from neutral-current interactions. Single-ring sub-GeV samples are divided into zero decay electrons and  $>$  zero decay electrons for  $e$ -like, and zero decay electrons, one decay electrons, and  $>$  one decay electrons for  $\mu$ -like, where the decay electrons are the number of delayed electrons reconstructed from the decay of charged pions and muons in the event.

An additional single-ring sub-GeV  $\pi^0$ -like sample is defined for  $e$ -like events passing a  $\pi^0$  cut, accounting for a fraction of neutral-current events producing a  $\pi^0$  which decays to a pair of photons, but only one of them is reconstructed. For these events, another sample is defined in the case where both photons are reconstructed, sub-GeV two-ring  $\pi^0$ -like. Single-ring multi-GeV  $e$ -like events follow the same criteria as their sub-GeV counterparts, and no further classification is done for  $\mu$ -like events. Finally, for multiring multi-GeV  $e$ -like events, a two-step classification is done. The first one tags most of the neutral-current events into the multiring other sample. The remaining events are divided into neutrino and anti-neutrino samples.

As expected from Sec. V, sub-GeV samples are those most sensitive to the  $CP$ -violating phase. The effect from different values of  $\delta_{CP}$  in the most relevant samples is shown in Fig. 13. Additionally, in Fig. 13 we also show the power of multi-GeV  $e$ -like samples to discern between normal and inverted orderings. Despite their name,  $\bar{\nu}$ -like

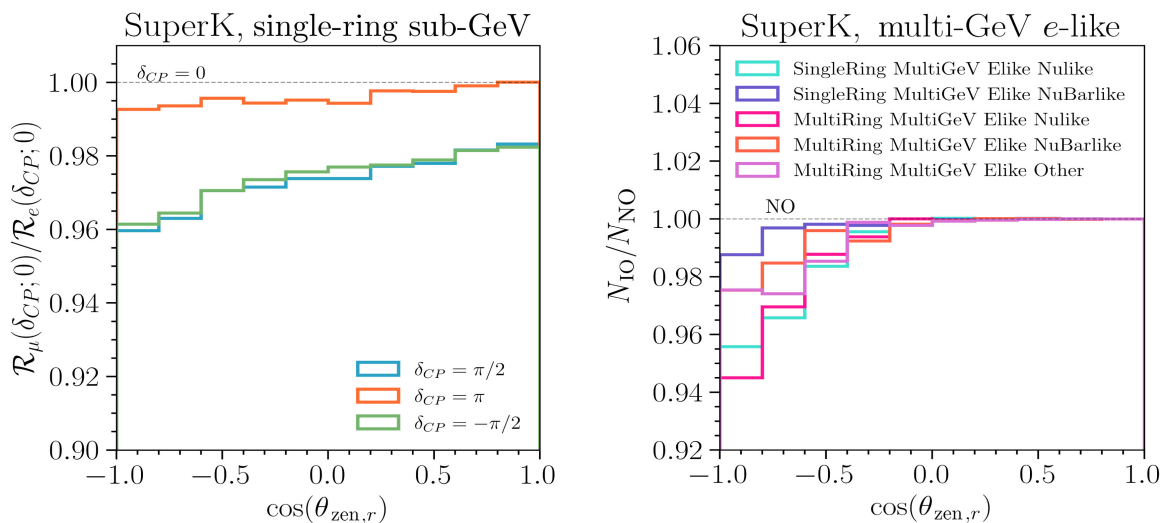


FIG. 13. Impact of different values of  $\delta_{CP}$  (left) and both neutrino mass orderings (right) for the most sensitive SuperK samples. On the left,  $\mathcal{R}_{\mu/e}(\delta_{CP};0)$  are the ratio of the number of events in sub-GeV  $\mu$ -like and  $e$ -like samples, with one and zero decay electrons, respectively, for a given value of  $\delta_{CP}$  compared with the case of  $\delta_{CP} = 0$ . On the right, we show the ratio between inverted ( $N_{IO}$ ) and normal ( $N_{NO}$ ) orderings for the number of events in SuperK single-ring and multiring multi-GeV  $e$ -like samples. The rest of the parameters follow Table III.

samples have still more neutrinos than antineutrinos; this contamination of neutrinos is due to the modest neutrino-antineutrino separation power and the smaller  $\bar{\nu}$  cross section. Therefore, the effects of different values of  $\delta_{CP}$  or mass ordering scenarios are diluted. More details about the SuperK simulation can be found in the Supplemental Material [38].

Detector systematics have a secondary effect on the sensitivity to the oscillation parameters, except  $\delta_{CP}$ , as compared with those of the flux or the neutrino-nucleon cross section. To realistically assess the sensitivity of the experiment, we implement a subset of the most relevant SuperK detector systematic uncertainties as detailed as possible within the reach of our simulation. Our implemented systematics follow Ref. [47] and are summarized in Table IV for each of the three major detector phases aforementioned.

### B. Super-Kamiokande with neutron tagging

After the electronics upgrade in 2008, SuperK was able to lower the signal threshold enough to be sensitive to the 2.2-MeV gamma from the deexcitation of deuterium after neutron capture on hydrogen. Despite being very weak, this signal is reconstructed with an efficiency of approximately 20%.

Further, in 2018, the upgrade of the SuperK detector started to make it compatible with dissolving Gd. At 0.2% concentration by mass of Gd sulfate in water, 90% of the thermal neutrons are captured by Gd with a half-life of approximately 30  $\mu$ s, emitting an 8-MeV  $\gamma$  cascade. This is detected by SuperK with an efficiency of 90%, having a final neutron-tagging efficiency of approximately 80%. Currently, SKGd is running at a third of the goal

TABLE IV. Summary of the SuperK detector systematic uncertainties used in this work.

Systematic source	$1\sigma$ range (SuperK-I to III)	$1\sigma$ range (SuperK-IV SKGd)
Energy scale	3%	2%
FC-PC separation	6%	0.2%
FC reduction	0.3%	2%
Fiducial volume	2%	1.3%
PC reduction	3.5%	1%
SubGeV2ringPi0	6%	6%
SubGeV1ringPi0	25%	15%
Multiring $\nu - \bar{\nu}$	6%	3%
Multiring other	6%	4%
PC-stop PC-thru	25%	20%
$\pi^0$ ring separation	2%	2%
$e$ -like ring separation	6%	2%
$\mu$ ring separation	3%	2%
Single-ring PID	0.35%	0.35%
Multiring PID	4%	4%
Decay- $e$ tag. eff.	10%	10%

gadolinium concentration, which is expected to be achieved in the next years [191].

Neutrinos produce on average fewer neutrons than antineutrinos; then, in addition to the usual cut in the number of electrons from muon decays for single-ring samples, a cut is applied in the number of tagged neutrons (zero neutrons or  $\geq$  one neutron) to improve the neutrino-antineutrino separation. This establishes new sample definitions for the analysis of SuperK-IV data.

The SuperK atmospheric neutrino analysis includes this neutron information by defining new event samples to improve the separation between neutrinos and antineutrinos. The previously explained single-ring  $e$ -like events with zero decay electrons are divided into samples with zero tagged neutrons or one or more tagged neutrons, and similarly, for  $\mu$ -like events as described in Ref. [192].

This improved event classification enhances the sensitivity to those oscillation parameters behaving differently for neutrinos and antineutrinos, namely, the  $CP$  phase and the neutrino mass ordering. These effects are shown in Fig. 14 for the case of Gd-neutron tagging.

### C. Hyper-Kamiokande

HyperK is a next-generation water-Cherenkov neutrino and proton-decay experiment in Japan expected to take over the current SuperK detector in 2027. It will be a scaled-up version of SuperK consisting of a cylinder of 74 m in diameter and 60 m in height, with a total mass of 258 kt [28]. The detector design is very similar to that of SuperK, with inner and outer detectors, the fiducial volume is 187 kt, a factor 8.4 larger than that of SuperK. The inner detector will be instrumented with approximately 20 000 20-in. PMTs and approximately 1000 additional multi-PMT modules [193,194]. The photo coverage will be 20%, which is half of SuperK, but the performance is expected to be better due to improved photosensors.

Given the similarities between SuperK and HyperK, we use our SK-Htag simulation as the baseline Monte Carlo for HyperK. This assumption provides a conservative estimate of the detector sensitivity as preliminary studies have already shown that neutron tagging on hydrogen will be more efficient in HyperK than in SuperK; see Refs. [195,196].

In the analysis, the HyperK simulated dataset is divided into the same samples as the SK-Htag, using 2 times the binning in zenith angle to account for the larger statistics. Following the same logic, we conservatively assume the same detector systematic errors as in for SuperK-IV, Table IV.

### D. IceCube and the IceCube Upgrade

IceCube is a 1-km<sup>3</sup> ice-Cherenkov detector located at the South Pole [197], consisting of 5160 digital optical modules (DOMs) deployed at depths between 1450 and 2450 m in the Antarctic glacier. The detector can observe neutrino

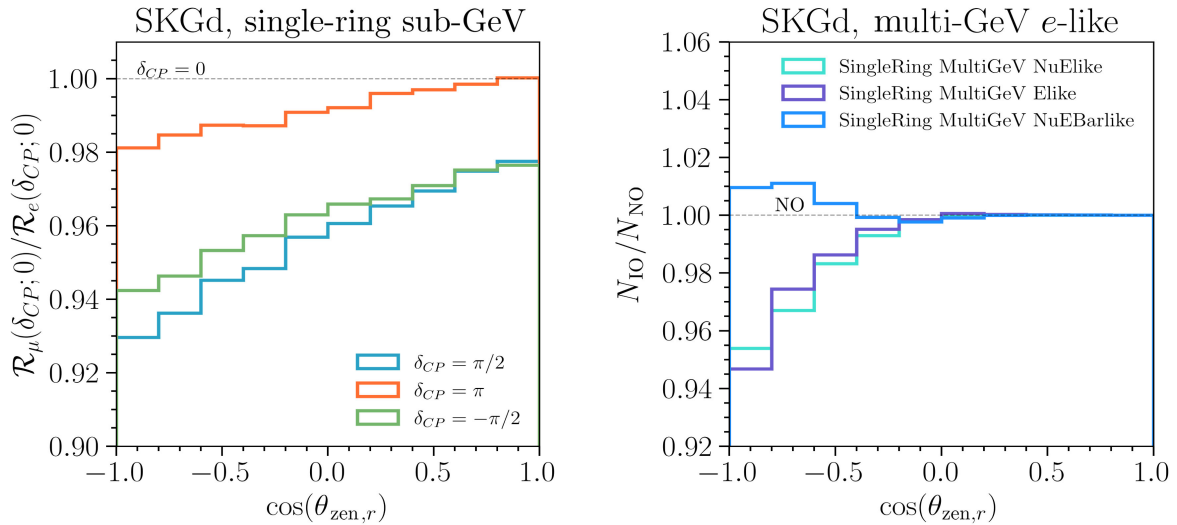


FIG. 14. Impact of different values of  $\delta_{CP}$  (left) and both neutrino mass orderings (right) for the most relevant SKGd samples. On the left,  $\mathcal{R}_{\mu/e}(\delta_{CP}; 0)$  are the ratio of the number of events in sub-GeV  $\mu$ -like and  $e$ -like samples, with zero Gd-tagged neutrons, and one and zero decay electrons, respectively, for a given value of  $\delta_{CP}$  compared with the case of  $CP$  conservation. On the right, we show the ratio between inverted ( $N_{IO}$ ) and normal ( $N_{NO}$ ) orderings for the number of events in SKGd single-ring multi-GeV  $e$ -like samples. The rest of the parameters follow Table III.

interactions with energies beyond approximately 10 GeV. The low-energy part of the atmospheric spectra is measured by IceCube DeepCore (DeepCore), a denser subarray of strings in the inner part of the detector of approximately 10 Mton. For energies around 10 GeV, two event morphologies can be differentiated in the detector: tracks, which are generated by the propagation of muons through the ice, and cascades produced by the propagation of electrons, taus, hadronic cascades, or electromagnetic cascades.

As described in Sec. V, IceCube has contributed to the measurement of  $\Delta m_{31}^2$  and  $\sin^2 \theta_{23}$ . Using the first three years of data [68,198], the sensitivity obtained is  $\Delta m_{31}^2 = 2.55^{+0.12}_{-0.11} \times 10^{-3} \text{ eV}^2$  and  $\sin^2 \theta_{23} = 0.58^{+0.04}_{-0.13}$ . These results are systematically limited, and further evaluation of the detector response together with a larger data sample predicts a large improvement in the precision over those parameters.

IceCube is planning an upgrade [199–201] that will consist of the deployment of additional strings to increase the total volume, leading to a large sample size with an increased energy range that will extend to lower energies. The upgrade will also increase the number of strings in the volume surrounding DeepCore, reducing the separation between the optical sensors and lowering the energy threshold to approximately 1 GeV. The new range of energies will increase the total amount of events observed thanks to the soft energy spectra of the atmospheric neutrino flux, as we can see in Fig. 15. The cascade sample dominates the low-energy sample due to the larger detector response at low energies.

The upgraded detector will be able to accurately explore the atmospheric parameters ( $\Delta m_{31}^2$ ,  $\sin^2 \theta_{23}$ ). In Fig. 15, we

show the impact that several values of the mixing parameters have on the event distribution for  $\cos \theta \in [-1, -0.8]$ . In the two upper figures, we see the impact that  $\Delta m_{31}^2$  will have on the cascade (left) and track (right) distributions. As we see from that figure, the main sensitivity comes from tracks with reconstructed energy around 20 GeV, which coincides with the first minimum in the muon-disappearance channel. As we see in Fig. 15, tracks are sensitive to  $\sin^2 2\theta_{23}$ , and therefore can discriminate between maximal mixing and no maximal mixing, but have a very mild sensitivity to the octant.

The new range of energies accessible by the detector will bring the possibility of increasing the sensitivity over other parameters. As mentioned in Sec. V, neutrinos are sensitive to mass ordering at GeV due to Earth's matter effects. In Fig. 15, we see the event distribution for both mass orderings. The most significant difference is obtained for tracks with better angular resolution and energies below 10 GeV. At the GeV scale, enhancing the effective  $\tilde{\theta}_{13}$  leads to a significant effect in IceCube. At the bottom of Fig. 15, we see how two extreme values for  $\theta_{13}$  will modify the cascade and track distribution compared to the best-fit value measured in reactor experiments. The largest sensitivity comes from tracks with energies below approximately 20 GeV.

In the case of the IceCube upgrade, there is still not a dedicated analysis of the most relevant detector systematics uncertainties and their impact. For that reason, we use the same systematics as in the search for  $\nu_\tau$  carried out by DeepCore [68] extended to the lower energies of the upgrade. The detector uncertainties account for the different properties of the ice as optical absorption and scattering,

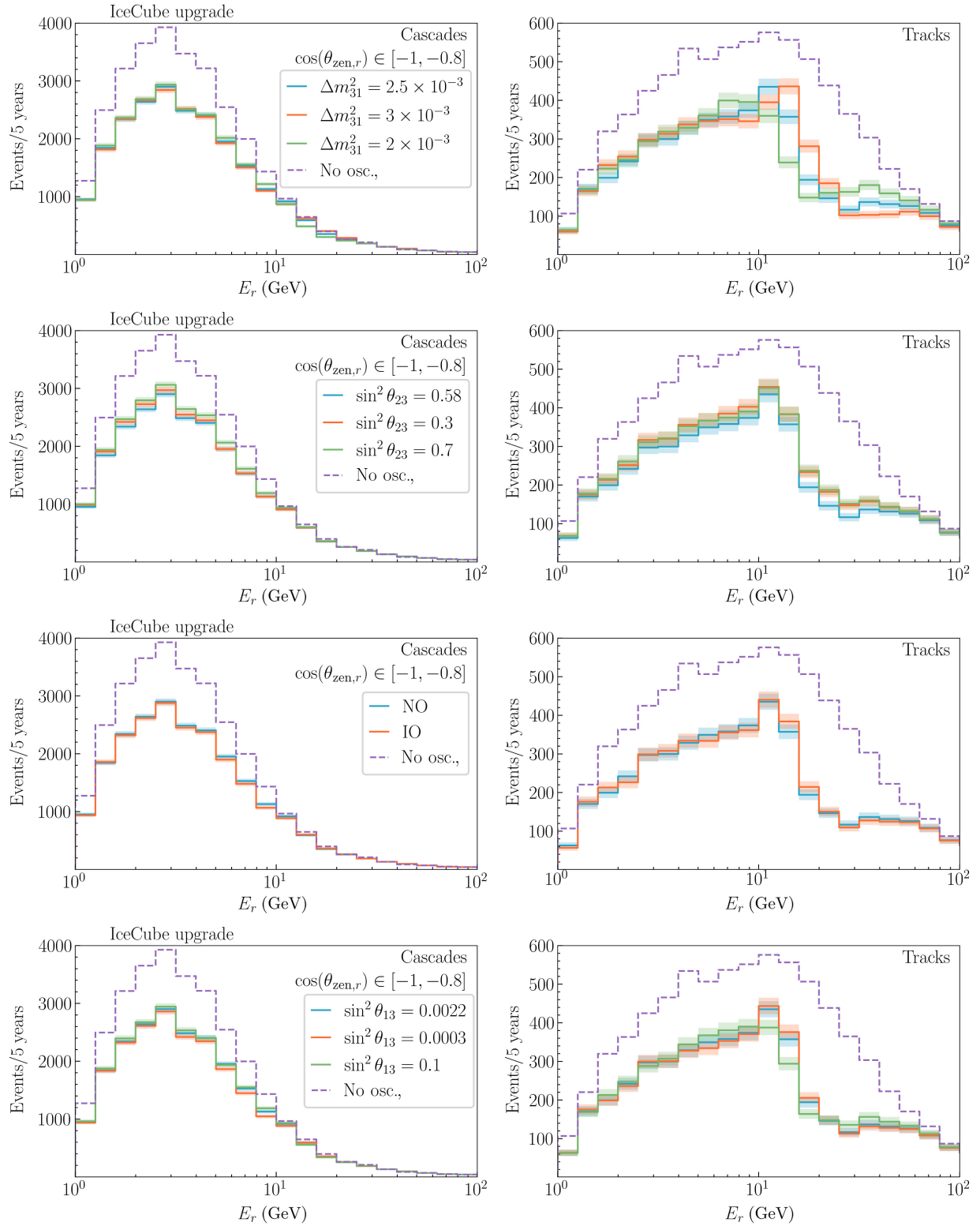


FIG. 15. Event distribution for different set of values of the mixing parameters for  $\cos \theta \in [-1, -0.8]$  as a function of the reconstructed neutrino energy ( $E_r$ ). We use the IceCube upgrade MC to evaluate the neutrino reconstructed energy [201]. The cascade distribution is shown on the left and tracks on the right. The statistical  $1\sigma$  error is shown as a band around the event distribution.

TABLE V. Summary of the IceCube Upgrade detector systematic uncertainties used in this work.

Systematic source	$1\sigma$ range
Ice absorption	10%
Ice scattering	10%
Overall optical efficiency	10%
Lateral optical efficiency	40%
Head-on optical efficiency	Free
Coin fraction	10%

the overall DOM efficiency, and the DOM response to lateral and head-on light. In Table V, we have a list of all the detector systematics used in this analysis and the  $1\sigma$  range.

### E. KM3Net and ORCA

A new water-Cherenkov neutrino telescope is under construction in the Mediterranean Sea, KM3NeT [202]. This experiment will be composed of two detectors: ARCA, a cubic kilometer water-Cherenkov detector that can observe high-energy neutrinos from the astrophysical sources in the northern sky, and ORCA, a megaton-scale experiment that will be able to explore the neutrino properties by measuring the atmospheric neutrino flux. In this article, we focus on the latter.

For this work, we develop an independent Monte Carlo for ORCA based on the IceCube Upgrade simulation that takes advantage of the event simulation carried out by the IceCube Collaboration. In the simulation of ORCA, we consider only events with reconstructed energy in the range of 1.85 to 53 GeV and keep the true neutrino variables from the IceCube simulation. Then, the reconstructed energy, reconstructed zenith, and event morphology are computed and assigned following the distributions in Ref. [203]. The Monte Carlo event weights for ORCA are translated from those of IceCube following the ratio of effective volumes between both experiments, as shown in Eq. (9),

$$w_{\text{MC}}^{\text{IC}} = A_{\text{eff}}^{\text{IC}} = V_{\text{eff}}^{\text{IC}} \sigma \frac{1}{n_d} = w_{\text{MC}}^{\text{ORCA}} \frac{V_{\text{eff}}^{\text{ORCA}}}{V_{\text{eff}}^{\text{IC}}}. \quad (9)$$

While the IceCube events are classified only into tracks and cascades, the ORCA Collaboration reports a more sophisticated event classification including a third (intermediate) class. To implement this, we reassign morphologies based on the results reported by the ORCA Collaboration in Ref. [203]. Further details of the development of the Monte Carlo simulation can be found in the Supplemental Material [38].

For the systematics treatment, we employ a similar set of systematics with the IceCube analysis. We use a same set of

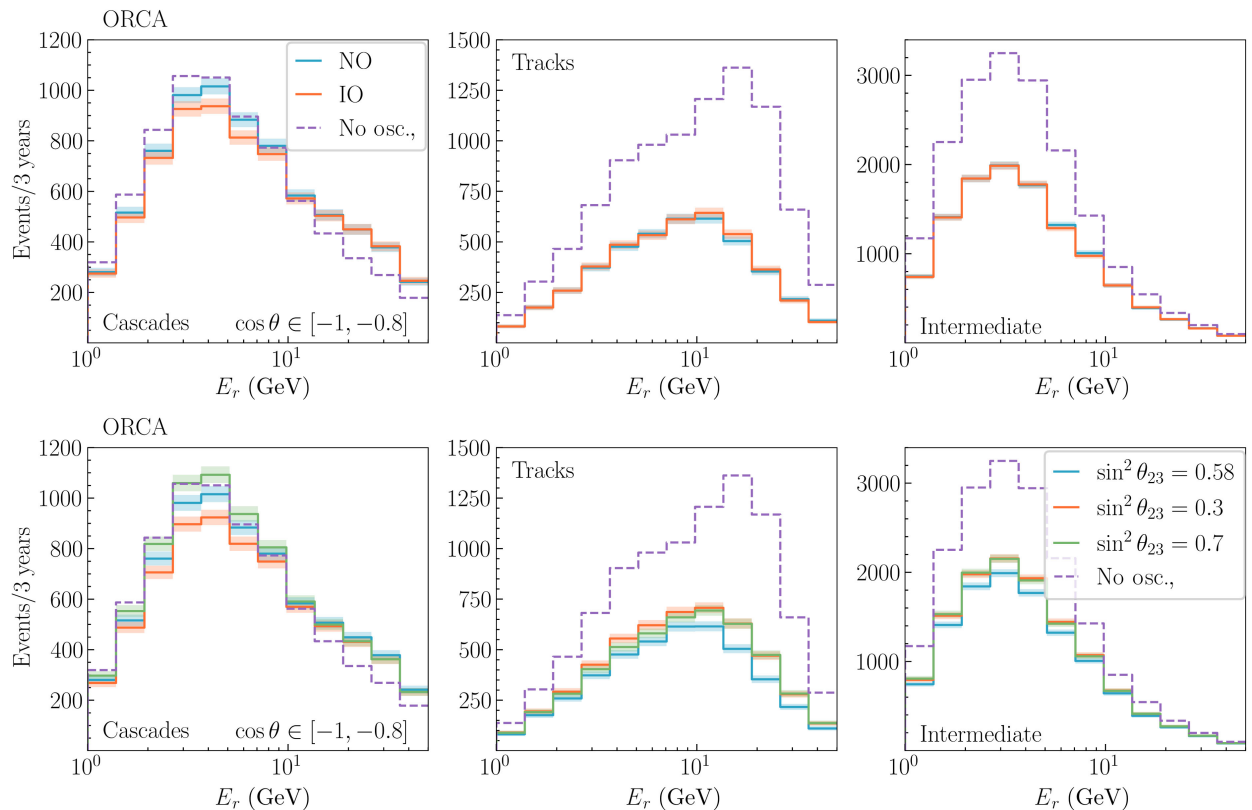


FIG. 16. Event distribution as a function of the reconstructed energy and direction for ORCA after three years of data taking. Lines correspond to event distributions (with oscillations) for track, cascade, and intermediate morphology classes, respectively.

TABLE VI. Summary of the ORCA detector systematic uncertainties used in this work.

Systematic source	$1\sigma$ range (ORCA)
Energy scale	5%
Intermediate	Free
Tracks	Free
Cascades	Free
Water absorption	10%
Water scattering	10%
Overall optical efficiency	10%
Lateral optical efficiency	40%
Head-on optical efficiency	10%

neutrino cross-section-related systematics: For the detector uncertainties, we assume the same electronics behaviors including DOM efficiency rates, and we adapt the ice-related uncertainties to that of the water in the case of ORCA.

In Fig. 16, we show the event distribution in reconstructed energy for both orderings (top) and for three different values of  $\sin^2 \theta_{23} = \{0.3, 0.58, 0.7\}$ . Worth noting is that intermediate events dominate the sample for the whole energy range. The new event morphology improves the “purity” in the cascade and track samples. The neutrino mass ordering changes the number of cascades with energies around the atmospheric resonance; Fig. (16) (top). Also, the normalization of the cascade sample contributes to the measurement of  $\sin^2 \theta_{23}$ . The same happens for tracks with energies around 5 GeV. For energies above approximately 10 GeV, tracks are sensitive to  $\sin^2 2\theta_{23}$ , which helps in the separation of  $\theta_{23}$  being maximal mixing or not.

In addition to the uncertainties related to the flux and the cross section, the measurement carried out in ORCA will be also affected by the uncertainties in the detector response. We consider a free normalization for each of the event morphologies used in the analysis and a 5% error on the energy scale, Table VI. Additionally, in line with the IceCube methodology for addressing detector uncertainties, we incorporate a set of systematic factors to consider the absorption and scattering of photons in water, as well as the response of the photomultiplier.

## F. DUNE

Liquid-argon time projection chamber (LArTPC) detectors have demonstrated a good capacity in the reconstruction of sub-GeV neutrinos. The energy and direction of the incoming neutrino can be reconstructed by detecting the tracks of all charged particles produced after the neutrino interaction and identifying them by their topology and energy loss. DUNE is planning to use a 20-kton detector based on this technology to reconstruct beam neutrinos, although they can also measure the atmospheric neutrino flux.

The reconstruction of the sub-GeV atmospheric neutrinos give us access to determine the  $CP$  phase. Following Ref. [149], the event distribution in the reconstructed energy and direction has been estimated by a simulation of the neutrino-argon interaction using an event generator. The uncertainties considered for the outgoing protons are 10% in energy and  $10^\circ$  in the direction. In the case of the leptons, we use 5% for the energy and  $5^\circ$  for the direction. Because of the LArTPC capabilities in identifying low-energy charged particles, the events are classified by the number of outgoing visible protons. This allows a statistical separation between neutrinos, which dominates the fraction of the sample with one proton, and antineutrinos, which dominate the zero-proton sample.

Considering a 20-kton detector, taking data for one year, we get a sensitivity over  $\delta_{CP}$  around  $1.5\sigma$ ; Fig. 17. In this analysis, we include only the uncertainties related to the flux and the detector response. Another set of uncertainties related to the neutrino-argon cross section will also affect this sensitivity. The low number of events expected by the end of this decade, and the large uncertainties, means that the DUNE measurement of the atmospheric neutrino flux cannot contribute significantly to the determination of  $\delta_{CP}$  by the end of this decade. Therefore, we decide not to include this measurement in our analysis.

## VII. RESULTS

In our analysis, we explore the combined sensitivity that the present and near-future generation of atmospheric neutrino experiments will have in determining the oscillation parameters for the  $3\nu$  mixing scenario by the end of this decade. Through the simulation of the different phases of SuperK, IceCube Upgrade, and ORCA, and the inclusion of all the previously discussed systematic uncertainties (flux, cross section, and detector), we investigate the synergies between the three experiments for the sensitivity to the  $\Delta m_{31}^2$ ,  $\theta_{23}$ ,  $\delta_{CP}$ , and  $\theta_{13}$  oscillation parameters.

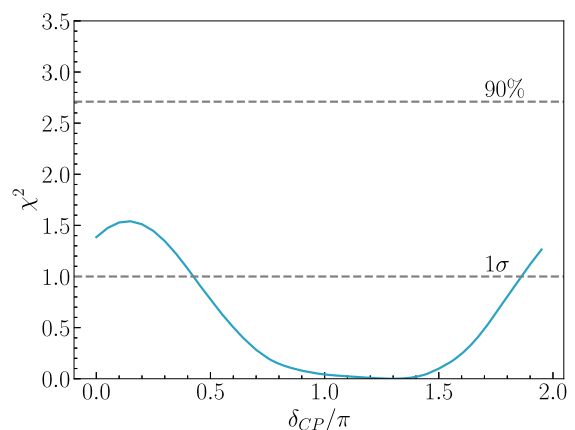


FIG. 17. DUNE sensitivity to  $\delta_{CP}$ . We consider one year of data taking and two modules of 10 kton each.

Unless otherwise stated, our study of the neutrino oscillation sensitivity presented here assumes the values and treatment shown in Table III.

For baselines comparable to Earth's diameter, neutrino oscillations are sizeable at  $E_\nu \sim 100$  GeV and lower. The location of the first oscillation minimum occurs at energies around 20 GeV and depends on the value of  $\Delta m_{31}^2$ . The amplitude of this oscillation is modulated by  $\sin^2 \theta_{23}$ . This energy region will be measured with large sample sizes by the IceCube Upgrade and ORCA. SuperK also has some sensitivity to this region from the multi-GeV multiring samples, but with smaller sample sizes. The track sample dominates the sensitivity to  $\Delta m_{31}^2$  thanks to better angular resolution. Since the atmospheric neutrino flux is dominated by  $\nu_\mu$ , tracks are mainly sensitive to  $P_{\mu\mu}$ .

On the other hand, as seen in Sec. V, the muon-disappearance channel is sensitive to  $\sin^2 2\theta_{23}$ , so it can distinguish only whether  $\sin^2 \theta_{23}$  is maximal mixing or not. To distinguish between both octants, we need to consider the appearance channel proportional to  $\sin^2 \theta_{23}$ . Water detectors have a better angular resolution compared to ice detectors due to the larger number of direct photons arriving at the PMTs. For that reason, ORCA, SuperK, and HyperK show a better precision for  $\sin^2 \theta_{23}$ . The combined analysis of the three experiments shows that  $\Delta m_{31}^2$  can be measured at approximately 0.6%, and the octant of  $\sin^2 \theta_{23}$  can be resolved at more than  $3\sigma$  in the assumed scenario. Fig. 18 shows that  $\Delta m_{31}^2$  is dominated by the IceCube Upgrade due to its better energy resolution; see Sec. VID.

At the GeV scale, neutrinos crossing the mantle undergo a large flavor oscillation due to the MSW resonance at

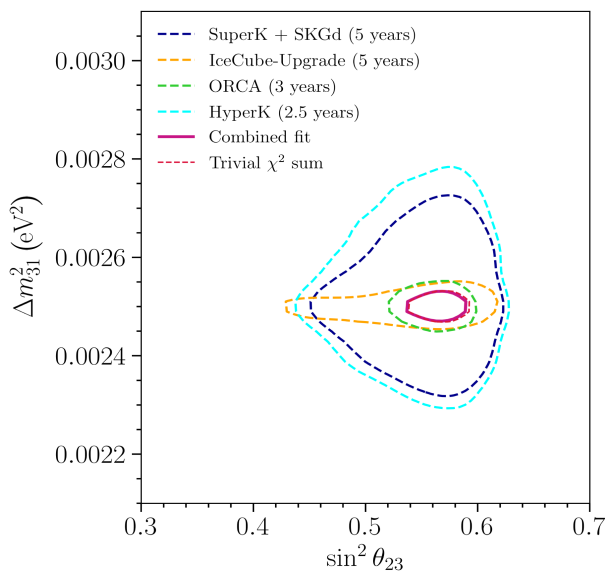


FIG. 18. Two-dimensional 90% confidence level regions for  $\sin^2 \theta_{23}$  and  $\Delta m_{31}^2$  for SuperK (dashed dark blue), IceCube Upgrade (dashed orange), ORCA (dashed green), HyperK (dashed cyan), and combined analysis (solid violet-red).

approximately 6 GeV. As described in Sec. V, the resonance happens due to the effective enhancement of the  $\theta_{13}$  mixing angle. This affects neutrinos if the mass ordering is normal, and antineutrinos in the inverted scenario. Although atmospheric experiments cannot differentiate between neutrinos and antineutrinos on an event-by-event basis, the differences in the flux and the cross section allow for statistical separation. Since this is a very localized process in energy and direction, the events with better angular and energy resolution will contribute more to identifying it, and therefore, they will contribute to the neutrino mass ordering sensitivity. This is what we observe in Fig. 15, where tracks show a larger modification under the mass ordering. For the case of HyperK, SuperK, and ORCA, we see in Figs. 13, 14, and 16, respectively, that most of the sensitivity to the ordering comes from  $e$ -like and cascades samples in the relevant energy region. In Fig. 3, we show the sensitivity to the ordering as a function of the operation time by combining the three experiments. It would be possible to obtain a  $6\sigma$  identification of the ordering after five years of SuperK with Gd in addition to its current exposure, five years of IceCube Upgrade, and three years of ORCA even with the obtained 90% CL range over  $\sin^2 \theta_{23}$ .

The effective enhancement on  $\theta_{13}$  also provides the option to measure this parameter. Although this parameter has been measured with high precision in reactor experiments [134,135,204] looking for the disappearance of  $\bar{\nu}_e$  and more recently in LBL [46,205] using the appearance channel, atmospheric neutrinos bring us a complementary way to measure it via the matter effect in Earth. Also, this will constitute the first observation of the MSW effect on Earth. This parameter is measured by the three experiments separately, and the combined analysis will reach an uncertainty smaller than 20%; see Fig. 19.

Finally, the  $CP$  phase is the least constrained parameter, for which almost the entire range is allowed at  $3\sigma$ ; T2K [24] and NO $\nu$ A [25] are the only experiments that have shown some sensitivity. So far, the only atmospheric measurement that shows some sensitivity over  $\delta_{CP}$  comes from SuperK [43], which excludes values around  $\delta_{CP} = \pi/5$  with a significance slightly above  $2\sigma$ . This parameter is the main target for the next-generation neutrino experiments. Using the presented atmospheric experiments, the sensitivity over some parameter values can be increased up to 99% CL; see Fig. 20. Still, the sensitivity is dominated by SuperK and HyperK, but IceCube and ORCA can get a  $1\sigma$  significance thanks to their low-energy measurements. The  $\delta_{CP}$  is the parameter that benefits the most from the combined analysis due to the large sample sizes from the IceCube Upgrade and ORCA constraining additionally the flux uncertainties which reduce the sensitivity to this parameter.

Previous studies such as the ones given in Refs. [9,146,206] do not consider the correlation between systematic uncertainties as we have done in this work. The improved methodology provides enhanced capacity to

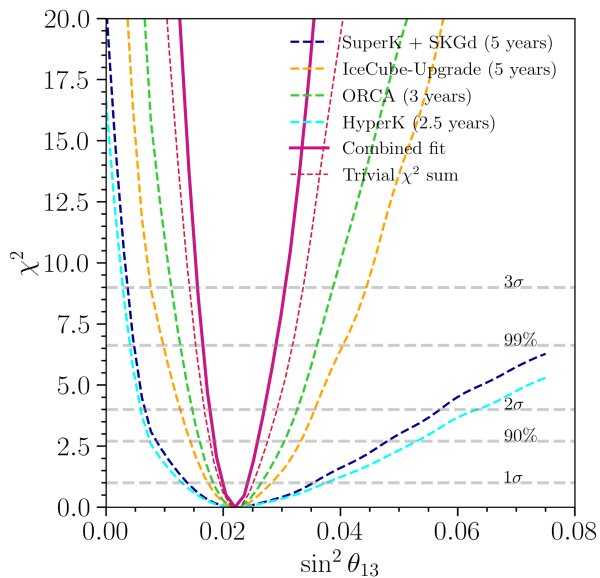


FIG. 19. Sensitivity to  $\sin^2 \theta_{13}$  for SuperK (dashed dark blue), IceCube Upgrade (dashed orange), ORCA (dashed green), HyperK (dashed cyan), and combined analysis (solid violet red).

determine  $\delta_{CP}$  and  $\theta_{23}$ , and has a lesser effect in other parameters. Throughout this work, the lines labeled “combined fit” and “trivial  $\chi^2$  sum” name our analysis and a simplified uncorrelated work, respectively. The difference between these two lines showcases the impact of the correlated systematics.

The excluded region for  $\delta_{CP}$  depends on its true value because it predicts very different event distributions for electron and muon samples in SuperK and HyperK, and also, it modifies the cascade (and intermediate events) distribution in the case of IceCube Upgrade (ORCA). Since

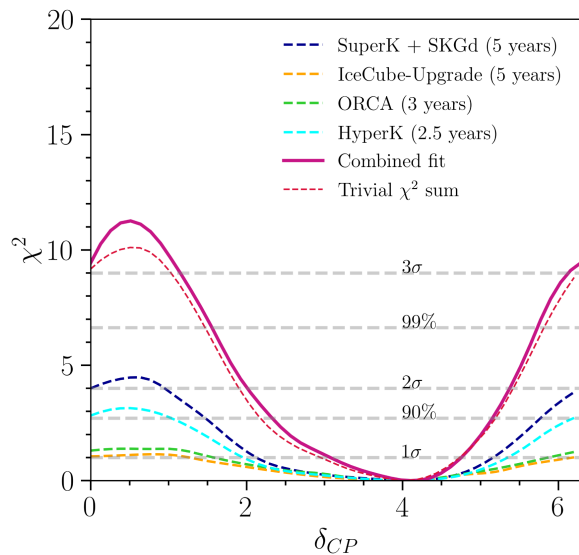


FIG. 20. Sensitivity to  $\delta_{CP}$  for SuperK (dashed dark blue), IceCube Upgrade (dashed orange), ORCA (dashed green), HyperK (dashed cyan), and combined analysis (solid violet red).

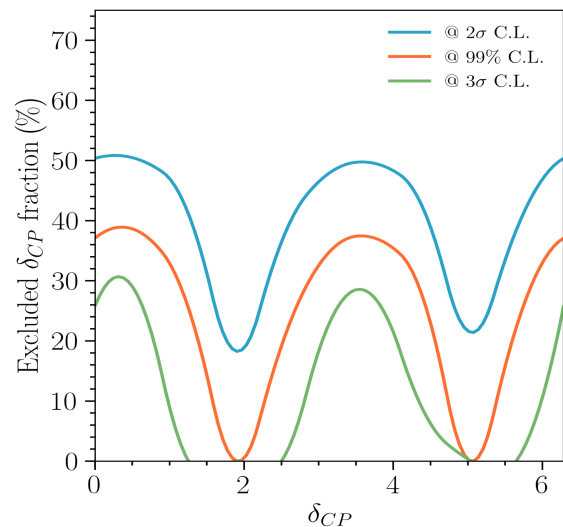


FIG. 21. Excluded fraction of  $\delta_{CP}$  as a function of the true value of  $\delta_{CP}$ . Lines correspond to exclusion at  $2\sigma$  (blue), 99% (orange), and  $3\sigma$  (green) for the combined fit assuming normal ordering and fixed  $\sin^2 \theta_{13} = 0.022$ . 40% of the parameter space can be excluded at 99% confidence level for the  $CP$ -conserving scenario. For lower confidence levels, the small deviations in the event number expectations can contribute to increase the sensitive region making the sensitivity more uniform.

almost the entire space is allowed, we explore what fraction of  $\delta_{CP}$  can be excluded at some confidence levels and for different true values of  $\delta_{CP}$ ; see Fig. 21. The most favorable scenario would correspond to  $\delta_{CP} = 0$  or  $\pi$ , where 60% of the whole space can be excluded at 90% CL, and a significant portion, 30% of the space, is excluded with a significance greater than  $3\sigma$ .

In Table VII, we summarize the projected  $1\sigma$  regions for all four oscillation parameters considered free in this combined analysis and with the true values from Table III.

## VIII. DISCUSSION AND OUTLOOK

Atmospheric neutrinos have played a very important role in determining the oscillation parameters since they were observed by SuperK [175]. As we highlight in this article, the large range of energies and baselines covered by the flux crossing Earth leads to a great sensitivity in the determination of the atmospheric parameters ( $\Delta m_{31}^2$  and  $\theta_{23}$ ). The matter effect at the GeV scale on neutrinos

TABLE VII.  $1\sigma$  sensitivity range from the combined analysis of the atmospheric neutrino experiments.

Parameter	$1\sigma$ range
$\sin^2 \theta_{13}$	[0.0199, 0.0242]
$\sin^2 \theta_{23}$	[0.554, 0.578]
$\delta_{CP}$	[3.12, 4.74]
$\Delta m_{31}^2$ (eV <sup>2</sup> )	[0.002487, 0.002514]

crossing the core and the mantle also brings the possibility of measuring the mass ordering and the so-called reactor angle ( $\theta_{13}$ ). Finally, at the GeV scale and below, the deviations in the appearance channel and statistical differentiation between neutrinos and antineutrinos allow the constraint of the  $CP$ -violation phase.

The results obtained in our analysis indicate that soon, atmospheric neutrinos can provide a complementary role in constraining the oscillation parameters and improving, in some cases, the precision obtained by long-baseline experiments. For instance, in the case of mass ordering, the combined analysis of LBL has a  $2\sigma$  preference for inverted ordering due to the tension in  $\delta_{CP}$  [207], while the latest results from atmospheric neutrinos show a preference for normal ordering with a significance larger than  $2\sigma$  [43]. The results presented in this study demonstrate that atmospheric neutrinos alone are poised to achieve a significance exceeding  $6\sigma$ . This suggests that these parameters will be measured with remarkable precision by the conclusion of this decade, as illustrated in Fig. 3.

The measurement of the atmospheric parameters is currently dominated by LBL experiments. In the case of  $\Delta m_{31}^2$ , the current sensitivity is dominated by T2K [208] and NO $\nu$ A [205], and it is known with an accuracy of approximately 1.1% [146] according to the latest global analysis. The sensitivity to this parameter can be largely improved up to approximately 0.5% using just atmospheric neutrinos. The latest results on  $\sin^2 \theta_{23}$  indicate a preference for the upper octant at a significance smaller than  $1\sigma$ , and maximal mixing is excluded with less than  $2\sigma$  significance. If we assume the current best-fit value of the global analyses, atmospheric neutrinos can achieve a  $3\sigma$  sensitivity over maximal mixing, ruling out the lower octant with a higher significance than the LBL experiments, as shown in Fig. 22. These results predict that atmospheric neutrinos will rule out the wrong octant of  $\theta_{23}$  with a large significance by the end of the decade. Most of the sensitivity over those two parameters comes from the region above approximately 10 GeV dominated by the large sample size of IceCube Upgrade and ORCA measurements and, to a lesser extent, SuperK and HyperK. In that region, the event distribution is dominated by  $\nu_\mu$  that interacts via DIS. Therefore, flux and cross-section systematic uncertainties have a mild effect on the sensitivity as shown in Figs. 23 and 24.

Until now, the  $CP$ -violation phase has been explored with a low significance and, only a small region around  $\delta_{CP} = \pi/2$  is excluded at more than  $3\sigma$  [146]. By the end of the decade, a significant fraction of the parameter space will be excluded by atmospheric neutrinos, as shown in Fig. 21. That will also help in resolving the actual tension between T2K and NO $\nu$ A in the determination of  $\delta_{CP}$  and  $\sin^2 \theta_{23}$  [207] thanks to the possibility to differentiate between the two octants of  $\sin^2 \theta_{23}$ , as shown in Fig. 22.

We undertake a systematic study to examine how potential future improvements in various systematic

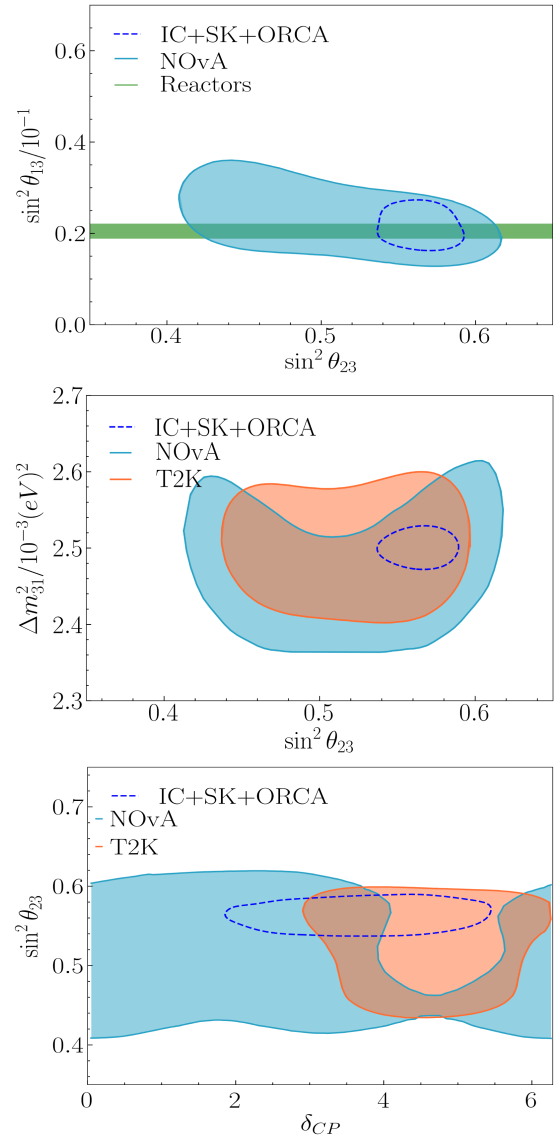


FIG. 22. Present sensitivity to the  $3\nu$  mixing parameters Comparison between the latest results from reactor and LBL measurements, and the future prediction from the combined analysis of SuperK, IceCube upgrade, and ORCA.

uncertainties will enhance sensitivity regarding that specific parameter. The sensitivity to the  $CP$  phase is heavily impacted by the uncertainties of the flux, detector, and, to a lesser extent, cross section; see Fig. 23. The flavor ratio and normalization below 1 GeV of the flux, and those related to the CCQE cross section, are the uncertainties reducing the sensitivity to this parameter. Detector systematics have a similar quantitative impact in the sensitivity as those of the flux. An independent and complementary to long-baseline experiments measurement of  $\delta_{CP}$  is of utmost importance to boost the precise picture of the three-flavor neutrino mixing. Ancillary measurements of the low-energy cosmic-ray flux and hadron production in proton and  ${}^4\text{He}$  scattering with nitrogen and oxygen nuclei, as well

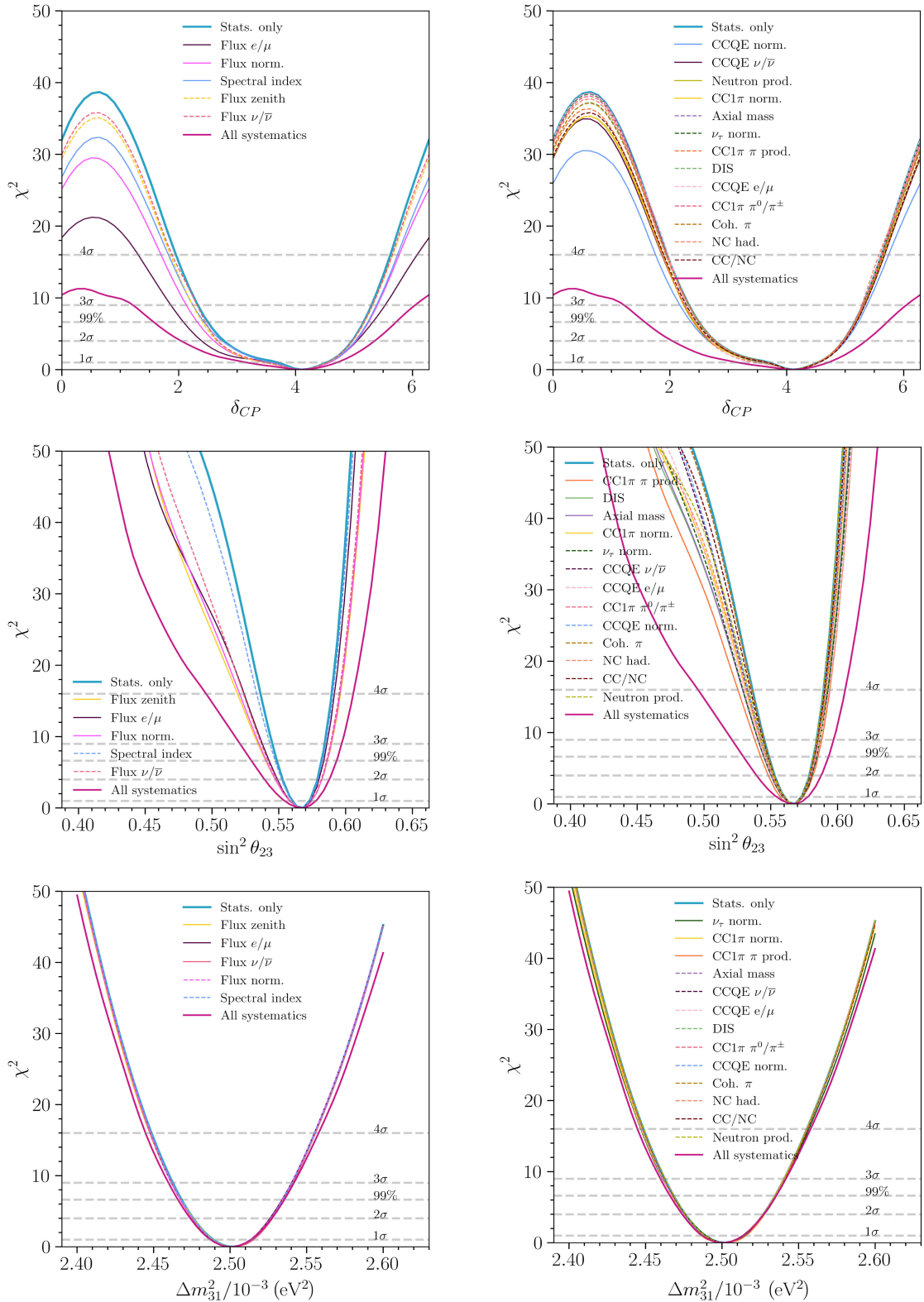


FIG. 23. From top to bottom, the impact of each atmospheric neutrino flux (left) and cross-section (right) systematic uncertainties on the sensitivity to  $\delta_{CP}$ ,  $\sin^2 \theta_{23}$ , and  $\Delta m_{31}^2$ . For clarity, solid lines represent the most relevant systematics, while dashed lines represent the rest.

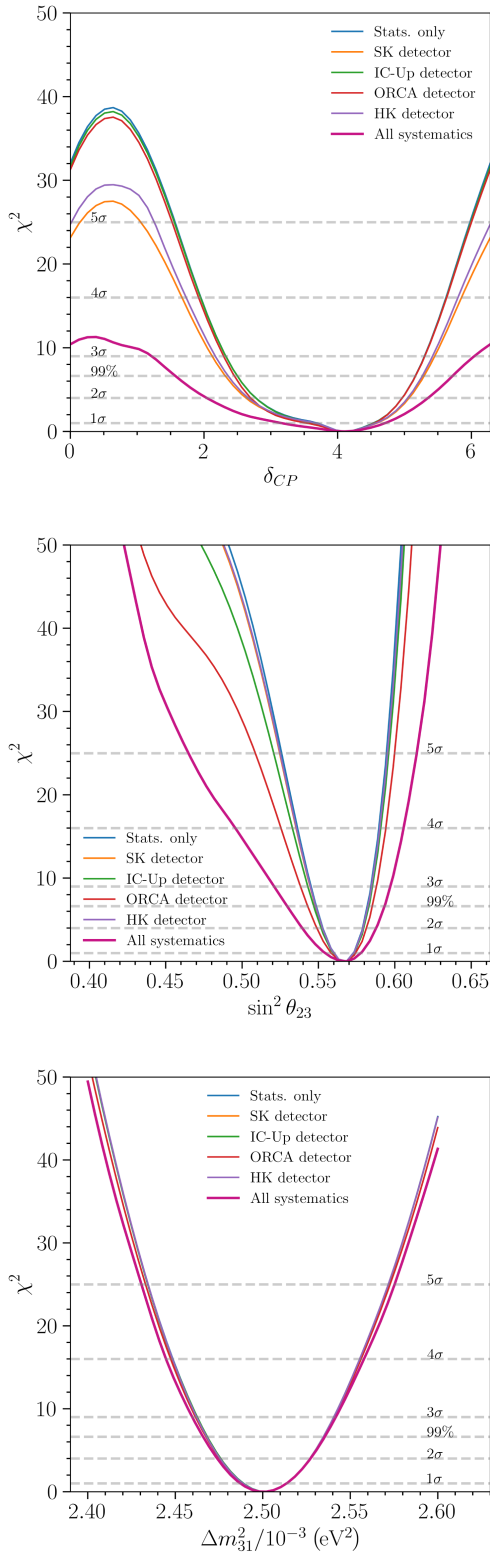


FIG. 24. From top to bottom, impact of each detector’s systematic uncertainties on the sensitivity to  $\delta_{CP}$ ,  $\sin^2 \theta_{23}$ , and  $\Delta m_{31}^2$ .

as development of more complete models, would narrow these uncertainties with a significant enhancement in the sensitivity to  $\delta_{CP}$  from atmospheric neutrinos. Further, as we discuss in Sec. III, the current and projected experiments for measuring the neutrino cross section below 1 GeV needed for next-generation accelerator neutrino experiments will provide valuable input for improving the measurement of the  $CP$  phase with atmospheric neutrinos.

Finally, the measurement of  $\theta_{13}$  is dominated by reactor experiments [134,135,204], but lately, LBL experiments have measured this parameter with a considerable precision [46,205]. We explore the possibility of measuring  $\theta_{13}$  in the atmospheric neutrino flux using the matter effects at the GeV scale. The results indicate that by the end of the decade, it will be possible to reach a 20% precision with the atmospheric neutrino flux; see Fig. 19. Although the precision is not comparable to the reactor measurements, it will certainly be on the same order as LBL measurement; Fig. 15. Exploring the mixing parameters at different energy scales might be a convenient way to search for new physics [209–214]. In addition, the resulting scenario also enables atmospheric neutrinos to play a prominent role in the measurement of the  $\nu_\tau$  cross section. Tau neutrinos are not expected from the unoscillated atmospheric flux, but they are measured in the detectors due to neutrino oscillations and strongly depend on the associated oscillation parameters. This way, such a combined analysis will provide very valuable input for the lower end of the charged-current  $\nu_\tau$  cross section; see the discussion in Refs. [215,216].

## IX. CONCLUSION

In this article, we explore the sensitivity of current and soon-to-operate water(ice)-Cherenkov atmospheric neutrino detectors—namely, IceCube Upgrade, ORCA, SuperK, and HyperK—to determine neutrino oscillation parameters. To simulate these experiments, we have developed dedicated Monte Carlo simulations and reproduce with good fidelity their experimental results. We incorporate more than 80 sources of systematic uncertainties and treat the correlated uncertainties among experiments, namely, those associated with the common cross section and flux. Through a comprehensive study, we motivate a combined data fit from these experiments by showing the few-percent-level precision that it would provide to the measurement of the remaining oscillation parameters—in particular,  $\theta_{23}$ ,  $\Delta m_{31}^2$ —and the neutrino mass ordering, as well as providing a constraint on the value of the  $CP$  phase independent from long-baseline neutrino experiments. Furthermore, the tools and the analysis presented in this work comprise the crucial first step to properly include atmospheric neutrinos in global fits.

Additionally, we identify the synergies among experiments and the common systematic uncertainties diminishing

the sensitivity for each parameter. We have an extended discussion of the sources of these uncertainties, in particular, regarding the flux and cross-section inputs. It is worth noting that while our analysis uses conservative estimations of the flux and cross-section uncertainties, both are expected to be improved through new measurements and further theoretical developments. In other words, this is a motivation for further ancillary measurements and methods, since an improved set of aforementioned estimations will greatly benefit the sensitivity of the analyzed experiments, and of particular relevance for the sensitivity to  $\delta_{CP}$ .

On the detector side, our analysis is also conservative. The reconstructions used for all the experiments considered in this work use traditional reconstruction techniques. These traditional techniques have been shown to underperform compared to new machine-learning-enhanced reconstruction methods, which show greater accuracy and improved execution time; see, e.g., Refs. [126,217]. Additionally, in the case of the IceCube Upgrade, the reconstruction used in this work does not take full advantage of the next-generation sensors which have improved light collection. Improvements are also expected for ORCA as the detector development proceeds. In summary, the detector systematics assumed in this work can be taken as a conservative baseline that is expected to improve as this decade unfolds.

Finally, we emphasize that the results from a combined fit of atmospheric neutrinos would provide a very valuable input for the next-generation neutrino physics program toward the precise measurement of the  $CP$ -violating phase in the lepton sector. This combined analysis nurtures itself from more than 40 years of global expertise and measurements of neutrino-water interactions paving the road for next-generation neutrino-water experiments such as Hyper-Kamiokande and IceCube-Gen2.

## ACKNOWLEDGMENTS

We thank Ali Kheirandish, Matheus Hostert, Pedro Machado, Michele Maltoni, Antoine Kouchner, Francis Halzen, Sergio Palomares-Ruiz, Alfonso Garcia-Soto, Luis Labarga, and Roger Wendell for useful discussions. C. A. A., I. M. S., and M. J. are supported by the Faculty of Arts and Sciences of Harvard University. P. F. is supported by the Department of Physics of the University of Liverpool and by the Donostia International Physics Center. Additionally, C. A. A. and I. M. S. are supported by the Alfred P. Sloan Foundation. We thank Jean DeMerit for carefully proofreading this manuscript.

---

[1] Paolo Lipari, *Atmospheric neutrinos: From the pioneering experiments to IMB and Kamiokande*, in *Proceedings of the International Conference on History of the Neutrino: 1930–2018* (2018), <http://neutrinohistory2018.in2p3.fr>.

- [2] Yusuke Koshio, *Observation of atmospheric neutrinos*, *Universe* **6**, 80 (2020).
- [3] R. Becker-Szendy, C. B. Bratton, D. Casper, S. T. Dye, W. Gajewski, M. Goldhaber, T. J. Haines, P. G. Halverson, T. Jones, D. Kielczewska *et al.*, *A search for muon-neutrino oscillations with the IMB detector*, *Phys. Rev. Lett.* **69**, 1010 (1992).
- [4] K. S. Hirata *et al.* (Kamiokande-II Collaboration), *Observation of a small atmospheric muon-neutrino/electron-neutrino ratio in Kamiokande*, *Phys. Lett. B* **280**, 146 (1992).
- [5] Y. Ashie *et al.* (Super-Kamiokande Collaboration), *Evidence for an oscillatory signature in atmospheric neutrino oscillation*, *Phys. Rev. Lett.* **93**, 101801 (2004).
- [6] André de Gouvêa, *Neutrino mass models*, *Annu. Rev. Nucl. Part. Sci.* **66**, 197 (2016).
- [7] L. Wolfenstein, *Neutrino oscillations in matter*, *Phys. Rev. D* **17**, 2369 (1978).
- [8] Ivan Esteban, M. C. Gonzalez-Garcia, Alvaro Hernandez-Cabezudo, Michele Maltoni, and Thomas Schwetz, *Global analysis of three-flavour neutrino oscillations: Synergies and tensions in the determination of  $\theta_{23}$ ,  $\delta_{CP}$ , and the mass ordering*, *J. High Energy Phys.* **01** (2019) 106.
- [9] P. F. de Salas, D. V. Forero, S. Gariazzo, P. Martínez-Miravé, O. Mena, C. A. Ternes, M. Tórtola, and J. W. F. Valle, *2020 global reassessment of the neutrino oscillation picture*, *J. High Energy Phys.* **02** (2021) 071.
- [10] M. G. Aartsen *et al.* (IceCube Collaboration), *Searching for eV-scale sterile neutrinos with eight years of atmospheric neutrinos at the IceCube Neutrino Telescope*, *Phys. Rev. D* **102**, 052009 (2020).
- [11] M. G. Aartsen *et al.* (IceCube Collaboration), *eV-scale sterile neutrino search using eight years of atmospheric muon neutrino data from the IceCube Neutrino Observatory*, *Phys. Rev. Lett.* **125**, 141801 (2020).
- [12] N. Fornengo, M. Maltoni, R. Bayo Tomas, and J. W. F. Valle, *Probing neutrino nonstandard interactions with atmospheric neutrino data*, *Phys. Rev. D* **65**, 013010 (2001).
- [13] Arman Esmaili and Alexei Yu. Smirnov, *Probing non-standard interaction of neutrinos with IceCube and DeepCore*, *J. High Energy Phys.* **06** (2013) 026.
- [14] Jordi Salvado, Olga Mena, Sergio Palomares-Ruiz, and Nuria Rius, *Non-standard interactions with high-energy atmospheric neutrinos at IceCube*, *J. High Energy Phys.* **01** (2017) 141.
- [15] M. C. Gonzalez-Garcia, Michele Maltoni, Ivan Martinez-Soler, and Ningqiang Song, *Non-standard neutrino interactions in the Earth and the flavor of astrophysical neutrinos*, *Astropart. Phys.* **84**, 15 (2016).
- [16] M. G. Aartsen *et al.* (IceCube Collaboration), *Search for nonstandard neutrino interactions with IceCube DeepCore*, *Phys. Rev. D* **97**, 072009 (2018).
- [17] R. Abbasi *et al.* (IceCube Collaboration), *All-flavor constraints on nonstandard neutrino interactions and generalized matter potential with three years of IceCube DeepCore data*, *Phys. Rev. D* **104**, 072006 (2021).
- [18] R. Abbasi *et al.* (IceCube Collaboration), *Strong constraints on neutrino nonstandard interactions from TeV-scale  $\nu_u$  disappearance at IceCube*, *Phys. Rev. Lett.* **129**, 011804 (2022).

- [19] P. S. Bhupal Dev *et al.*, *Neutrino non-standard interactions: A status report*, *SciPost Phys. Proc.* **2**, 001 (2019).
- [20] S. V. Demidov, *Bounds on non-standard interactions of neutrinos from IceCube DeepCore data*, *J. High Energy Phys.* **03** (2020) 105.
- [21] M. G. Aartsen *et al.* (IceCube Collaboration), *Neutrino interferometry for high-precision tests of Lorentz symmetry with IceCube*, *Nat. Phys.* **14**, 961 (2018).
- [22] M. C. Gonzalez-Garcia and Michele Maltoni, *Atmospheric neutrino oscillations and new physics*, *Phys. Rev. D* **70**, 033010 (2004).
- [23] Yusuke Koshio, Gabriel D. Orebi Gann, Erin O’Sullivan, and Irene Tamborra, *Snowmass 2021 topical group report: Neutrinos from natural sources*, arXiv:2209.04298.
- [24] K. Abe *et al.* (T2K Collaboration), *Improved constraints on neutrino mixing from the T2K experiment with  $3.13 \times 10^{21}$  protons on target*, *Phys. Rev. D* **103**, 112008 (2021).
- [25] M. A. Acero *et al.* (NO $\nu$ A Collaboration), *Improved measurement of neutrino oscillation parameters by the NO $\nu$ A experiment*, *Phys. Rev. D* **106**, 032004 (2022).
- [26] K. Abe *et al.* (Super-Kamiokande Collaboration), *Atmospheric neutrino oscillation analysis with external constraints in Super-Kamiokande I–IV*, *Phys. Rev. D* **97**, 072001 (2018).
- [27] R. Abbasi *et al.* (IceCube Collaboration), *Measurement of atmospheric neutrino mixing with improved IceCube DeepCore calibration and data processing*, *Phys. Rev. D* **108**, 012014 (2023).
- [28] K. Abe *et al.* (Hyper-Kamiokande Collaboration), *Hyper-Kamiokande design report*, arXiv:1805.04163.
- [29] A. Abud Abed *et al.* (DUNE Collaboration), *Low exposure long-baseline neutrino oscillation sensitivity of the DUNE experiment*, *Phys. Rev. D* **105**, 072006 (2022).
- [30] If neutrinos are Majorana particles, two additional phases are present in this matrix, but they are not observable via flavor oscillation; thus, we ignore them in the rest of the discussion.
- [31] Guido Altarelli and Ferruccio Feruglio, *Discrete flavor symmetries and models of neutrino mixing*, *Rev. Mod. Phys.* **82**, 2701 (2010).
- [32] Hajime Ishimori, Tatsuo Kobayashi, Hiroshi Ohki, Yusuke Shimizu, Hiroshi Okada, and Morimitsu Tanimoto, *Non-Abelian discrete symmetries in particle physics*, *Prog. Theor. Phys. Suppl.* **183**, 1 (2010).
- [33] M. Fukugita and T. Yanagida, *Baryogenesis without grand unification*, *Phys. Lett. B* **174**, 45 (1986).
- [34] M. Aker *et al.* (KATRIN Collaboration), *Direct neutrino-mass measurement with sub-electronvolt sensitivity*, *Nat. Phys.* **18**, 160 (2022).
- [35] M. Agostini *et al.* (GERDA Collaboration), *Improved limit on neutrinoless double- $\beta$  decay of  $^{76}\text{Ge}$  from GERDA Phase II*, *Phys. Rev. Lett.* **120**, 132503 (2018).
- [36] A. Gando, Y. Gando, T. Hachiya, A. Hayashi, S. Hayashida, H. Ikeda, K. Inoue, K. Ishidoshiro, Y. Karino, M. Koga *et al.* (KamLAND-Zen Collaboration), *Search for Majorana neutrinos near the inverted mass hierarchy region with KamLAND-Zen*, *Phys. Rev. Lett.* **117**, 082503 (2016); **117**, 109903(E) (2016).
- [37] Eleonora Di Valentino, Stefano Gariazzo, and Olga Mena, *Most constraining cosmological neutrino mass bounds*, *Phys. Rev. D* **104**, 083504 (2021).
- [38] See Supplemental Material at <http://link.aps.org/supplemental/10.1103/PhysRevX.13.041055> for Appendix A: Description of the methods employed to produce the Monte Carlo simulations for the Super-Kamiokande and Hyper-Kamiokande experiments, as well as, the basic event distributions and reproduction of the official results. Appendix B: Description of the methods employed to produce the Monte Carlo simulations for the ORCA experiment, as well as, the basic event distributions and reproduction of the official results. Appendix C: Study of the variation in sensitivity to the oscillation parameters assuming different scenarios of  $\theta_{23}$ .
- [39] KM3NeT and JUNO Collaborations, *Combined sensitivity of JUNO and KM3NeT/ORCA to the neutrino mass ordering*, *J. High Energy Phys.* **03** (2022) 55.
- [40] Babak Abi *et al.* (DUNE Collaboration), *DUNE Physics*, Report No. FERMILAB-PUB-20-025-ND, arXiv:2002.03005.
- [41] This significance and others quoted later in this work rely on the use of Wilk’s theorem. See Ref. [42] for an extended discussion on its regime of applicability and caveats, especially for the case of the ordering as a non-nested hypothesis.
- [42] Sara Algeri, Jelle Aalbers, Knut Dundas Morå, and Jan Conrad, *Searching for new phenomena with profile likelihood ratio tests*, *Nat. Rev. Phys.* **2**, 245 (2020).
- [43] Linyan Wan, *Atmospheric neutrino\_Super-K*, Zenodo (2022), 10.5281/zenodo.6694761.
- [44] A. B. Balantekin *et al.*, *Snowmass neutrino frontier: Neutrino interaction cross sections (NF06) topical group report*, Report No. FERMILAB-CONF-22-696-ND-SCD, arXiv:2209.06872.
- [45] Soebur Razzaque and A. Yu. Smirnov, *Super-PINGU for measurement of the leptonic CP-phase with atmospheric neutrinos*, *J. High Energy Phys.* **05** (2015) 139.
- [46] K. Abe *et al.* (T2K Collaboration), *Constraint on the matter–antimatter symmetry-violating phase in neutrino oscillations*, *Nature (London)* **580**, 339 (2020); **583**, E16 (2020).
- [47] K. Abe *et al.*, *Atmospheric neutrino oscillation analysis with external constraints in Super-Kamiokande I–IV*, *Phys. Rev. D* **97**, 072001 (2018).
- [48] T. K. Gaisser and M. Honda, *Flux of atmospheric neutrinos*, *Annu. Rev. Nucl. Part. Sci.* **52**, 153 (2002).
- [49] Hans Peter Dembinski, Ralph Engel, Anatoli Fedynitch, Thomas Gaisser, Felix Riehn, and Todor Stanev, *Data-driven model of the cosmic-ray flux and mass composition from 10 GeV to  $10^{11}$  GeV*, *Proc. Sci., ICRC2017* (2018) 533 [arXiv:1711.11432].
- [50] Anatoli Fedynitch, Felix Riehn, Ralph Engel, Thomas K. Gaisser, and Todor Stanev, *Hadronic interaction model SIBYLL 2.3c and inclusive lepton fluxes*, *Phys. Rev. D* **100**, 103018 (2019).
- [51] Anatoli Fedynitch and Matthias Huber, *Data-driven hadronic interaction model for atmospheric lepton flux calculations*, *Phys. Rev. D* **106**, 083018 (2022).

- [52] Rikard Enberg, Mary Hall Reno, and Ina Sarcevic, *Prompt neutrino fluxes from atmospheric charm*, *Phys. Rev. D* **78**, 043005 (2008).
- [53] Rhorry Gauld, Juan Rojo, Luca Rottoli, Subir Sarkar, and Jim Talbert, *The prompt atmospheric neutrino flux in the light of LHCb*, *J. High Energy Phys.* **02** (2016) 130.
- [54] Thomas K. Gaisser, Ralph Engel, and Elisa Resconi, *Cosmic Rays and Particle Physics*, 2nd ed. (Cambridge University Press, Cambridge, England, 2016).
- [55] M. Honda, M. S. Athar, T. Kajita, K. Kasahara, and S. Midorikawa, *Atmospheric neutrino flux calculation using the NRLMSISE-00 atmospheric model*, *Phys. Rev. D* **92**, 023004 (2015).
- [56] IceCube Collaboration, *NUFLUX: A library for calculating atmospheric neutrino fluxes* (2023), <https://github.com/icecube/nuflux>.
- [57] R. Abbasi *et al.* (IceCube Collaboration), *Measurement of the atmospheric neutrino energy spectrum from 100 GeV to 400 TeV with IceCube*, *Phys. Rev. D* **83**, 012001 (2011).
- [58] M. G. Aartsen *et al.* (IceCube Collaboration), *Measurement of the atmospheric  $\nu_e$  flux in IceCube*, *Phys. Rev. Lett.* **110**, 151105 (2013).
- [59] E. Richard *et al.* (Super-Kamiokande Collaboration), *Measurements of the atmospheric neutrino flux by Super-Kamiokande: Energy spectra, geomagnetic effects, and solar modulation*, *Phys. Rev. D* **94**, 052001 (2016).
- [60] Paolo Lipari, *The geometry of atmospheric neutrino production*, *Astropart. Phys.* **14**, 153 (2000).
- [61] T. Futagami *et al.* (Super-Kamiokande Collaboration), *Observation of the east-west anisotropy of the atmospheric neutrino flux*, *Phys. Rev. Lett.* **82**, 5194 (1999).
- [62] J. L. Marshall *et al.*, *Improving global analysis and forecasting with AIRS*, *Bull. Am. Meteorol. Soc.* **87**, 891 (2006).
- [63] Gabriel L. W. H. Collin, *Neutrinos, neurons and neutron stars: Applications of new statistical and analysis techniques to particle and astrophysics*, Ph.D. thesis, Massachusetts Institute of Technology, 2018.
- [64] Gabriel Collin, *An estimation of systematics for up-going atmospheric muon neutrino flux at the South Pole*, MIT, <https://dspace.mit.edu/handle/1721.1/98078>.
- [65] E. Richard, *Studies of the energy, azimuthal, and time spectra of the atmospheric neutrino flux at Super-Kamiokande*, Ph.D. thesis, 2015.
- [66] G. D. Barr, S. Robbins, T. K. Gaisser, and Todor Stanev, *Uncertainties in atmospheric neutrino fluxes*, *Phys. Rev. D* **74**, 094009 (2006).
- [67] Kevin J. Kelly, Pedro A. N. Machado, Ivan Martinez-Soler, and Yuber F. Perez-Gonzalez, *DUNE atmospheric neutrinos: Earth tomography*, *J. High Energy Phys.* **05** (2022) 187.
- [68] M. G. Aartsen *et al.* (IceCube Collaboration), *Measurement of atmospheric tau neutrino appearance with IceCube DeepCore*, *Phys. Rev. D* **99**, 032007 (2019).
- [69] N. J. Baker, P. L. Connolly, S. A. Kahn, M. J. Murtagh, R. B. Palmer, N. P. Samios, and M. Tanaka, *Total cross sections for  $\nu_\mu n$  and  $\nu_\mu p$  charged-current interactions in the 7-foot bubble chamber*, *Phys. Rev. D* **25**, 617 (1982).
- [70] D. S. Baranov *et al.*, *Deep inelastic neutrino interactions in bubble chamber skat at 2–30 GeV*, *Phys. Lett.* **81B**, 258 (1979).
- [71] O. Erriques *et al.*, *Strange particle production by anti-neutrinos*, *Phys. Lett.* **70B**, 383 (1977).
- [72] Artur M. Ankowski, Omar Benhar, Pilar Coloma, Patrick Huber, Chun-Min Jen, Camillo Mariani, Davide Meloni, and Erica Vagnoni, *Comparison of the calorimetric and kinematic methods of neutrino energy reconstruction in disappearance experiments*, *Phys. Rev. D* **92**, 073014 (2015).
- [73] Omar Benhar, Patrick Huber, Camillo Mariani, and Davide Meloni, *Neutrino–nucleus interactions and the determination of oscillation parameters*, *Phys. Rep.* **700**, 1 (2017).
- [74] Nina M. Coyle, Shirley Weishi Li, and Pedro A. N. Machado, *The impact of neutrino-nucleus interaction modeling on new physics searches*, *J. High Energy Phys.* **12** (2022) 166.
- [75] A. M. Ankowski, M. B. Barbaro, Omar Benhar, J. A. Caballero, Carlotta Giusti, Raúl González-Jiménez, G. D. Megias, and A. Meucci, *Estimate of the theoretical uncertainty of the cross sections for nucleon knockout in neutral-current neutrino-oxygen interactions*, *Phys. Rev. C* **92**, 025501 (2015).
- [76] Noemi Rocco, Alessandro Lovato, and Omar Benhar, *Comparison of the electromagnetic responses of  $^{12}\text{C}$  obtained from the Green's function Monte Carlo and spectral function approaches*, *Phys. Rev. C* **94**, 065501 (2016).
- [77] Daniel Simons, Noah Steinberg, Alessandro Lovato, Yannick Meurice, Noemi Rocco, and Michael Wagman, *Form factor and model dependence in neutrino-nucleus cross section predictions*, arXiv:2210.02455.
- [78] L. Ren *et al.* (MINERvA Collaboration), *Measurement of the antineutrino to neutrino charged-current interaction cross section ratio in MINERvA*, *Phys. Rev. D* **95**, 072009 (2017); **97**, 019902(E) (2018).
- [79] X. G. Lu *et al.* (MINERvA Collaboration), *Exploring neutrino–nucleus interactions in the GeV regime using MINERvA*, *Eur. Phys. J. Special Topics* **230**, 4243 (2021).
- [80] D. Ruterbories *et al.* (MINERvA Collaboration), *Simultaneous measurement of proton and lepton kinematics in quasielasticlike  $\nu\mu$ -hydrocarbon interactions from 2 to 20 GeV*, *Phys. Rev. Lett.* **129**, 021803 (2022).
- [81] D. Coplowe *et al.* (MINERvA Collaboration), *Probing nuclear effects with neutrino-induced charged-current neutral pion production*, *Phys. Rev. D* **102**, 072007 (2020).
- [82] A. Mislivec *et al.* (MINERvA Collaboration), *Measurement of total and differential cross sections of neutrino and antineutrino coherent  $\pi^\pm$  production on carbon*, *Phys. Rev. D* **97**, 032014 (2018).
- [83] O. Altinok *et al.* (MINERvA Collaboration), *Measurement of  $\nu_\mu$  charged-current single  $\pi^0$  production on hydrocarbon in the few-GeV region using MINERvA*, *Phys. Rev. D* **96**, 072003 (2017).
- [84] A. Rodriguez *et al.* (K2K Collaboration), *Measurement of single charged pion production in the charged-current interactions of neutrinos in a 1.3-GeV wide band beam*, *Phys. Rev. D* **78**, 032003 (2008).

- [85] R. Gran *et al.* (K2K Collaboration), *Measurement of the quasi-elastic axial vector mass in neutrino-oxygen interactions*, *Phys. Rev. D* **74**, 052002 (2006).
- [86] M. Hasegawa *et al.* (K2K Collaboration), *Search for coherent charged pion production in neutrino-carbon interactions*, *Phys. Rev. Lett.* **95**, 252301 (2005).
- [87] S. Nakayama *et al.* (K2K Collaboration), *Measurement of single  $\pi^0$  production in neutral current neutrino interactions with water by a 1.3-GeV wide band muon neutrino beam*, *Phys. Lett. B* **619**, 255 (2005).
- [88] O. Samoylov *et al.* (NOMAD Collaboration), *A precision measurement of charm dimuon production in neutrino interactions from the NOMAD experiment*, *Nucl. Phys. B* **876**, 339 (2013).
- [89] Q. Wu *et al.* (NOMAD Collaboration), *A precise measurement of the muon neutrino-nucleon inclusive charged current cross-section off an isoscalar target in the energy range  $2.5 < E_\nu < 40$  GeV by NOMAD*, *Phys. Lett. B* **660**, 19 (2008).
- [90] V Lyubushkin *et al.* (NOMAD Collaboration), *A study of quasi-elastic muon neutrino and antineutrino scattering in the NOMAD experiment*, *Eur. Phys. J. C* **63**, 355 (2009).
- [91] C. T. Kullenberg *et al.* (NOMAD Collaboration), *A search for single photon events in neutrino interactions*, *Phys. Lett. B* **706**, 268 (2012).
- [92] Y. Nakajima *et al.* (SciBooNE Collaboration), *Measurement of inclusive charged current interactions on carbon in a few-GeV neutrino beam*, *Phys. Rev. D* **83**, 012005 (2011).
- [93] K. Abe *et al.* (T2K Collaboration), *Measurement of the inclusive  $\nu_\mu$  charged current cross section on iron and hydrocarbon in the T2K on-axis neutrino beam*, *Phys. Rev. D* **90**, 052010 (2014).
- [94] K. Abe *et al.* (T2K Collaboration), *Measurement of  $\bar{\nu}_\mu$  and  $\nu_\mu$  charged current inclusive cross sections and their ratio with the T2K off-axis near detector*, *Phys. Rev. D* **96**, 052001 (2017).
- [95] K. Abe *et al.* (T2K), *First measurement of the  $\nu_\mu$  charged-current cross section on a water target without pions in the final state*, *Phys. Rev. D* **97**, 012001 (2018).
- [96] K. Abe *et al.* (T2K Collaboration), *Measurement of coherent  $\pi^+$  production in low energy neutrino-carbon scattering*, *Phys. Rev. Lett.* **117**, 192501 (2016).
- [97] K. Abe *et al.* (T2K Collaboration), *Measurement of neutrino and antineutrino neutral-current quasielasticlike interactions on oxygen by detecting nuclear deexcitation  $\gamma$  rays*, *Phys. Rev. D* **100**, 112009 (2019).
- [98] K. Abe *et al.* (T2K Collaboration), *Measurements of  $\bar{\nu}_\mu$  and  $\bar{\nu}_\mu + \nu_\mu$  charged-current cross-sections without detected pions or protons on water and hydrocarbon at a mean anti-neutrino energy of 0.86 GeV*, *Prog. Theor. Exp. Phys.* **2021**, 043C01 (2021).
- [99] K. Abe *et al.* (T2K Collaboration), *Simultaneous measurement of the muon neutrino charged-current cross section on oxygen and carbon without pions in the final state at T2K*, *Phys. Rev. D* **101**, 112004 (2020).
- [100] K. Abe *et al.* (T2K Collaboration), *First measurement of the charged current  $\bar{\nu}_\mu$  double differential cross section on a water target without pions in the final state*, *Phys. Rev. D* **102**, 012007 (2020).
- [101] K. Abe *et al.* (T2K Collaboration), *Measurement of double-differential muon neutrino charged-current interactions on  $C_8H_8$  without pions in the final state using the T2K off-axis beam*, *Phys. Rev. D* **93**, 112012 (2016).
- [102] K. Abe *et al.* (T2K Collaboration), *Measurement of inclusive double-differential  $\nu_\mu$  charged-current cross section with improved acceptance in the T2K off-axis near detector*, *Phys. Rev. D* **98**, 012004 (2018).
- [103] K. Abe *et al.* (T2K Collaboration), *Measurement of the inclusive electron neutrino charged current cross section on carbon with the T2K Near Detector*, *Phys. Rev. Lett.* **113**, 241803 (2014).
- [104] K. Abe *et al.* (T2K Collaboration), *Measurement of the charged-current electron (anti-)neutrino inclusive cross-sections at the T2K off-axis near detector ND280*, *J. High Energy Phys.* **10** (2020) 114.
- [105] A. R. Back *et al.* (ANNIE Collaboration), *Accelerator Neutrino Neutron Interaction Experiment (ANNIE): Preliminary results and physics phase proposal*, arXiv:1707.08222.
- [106] A. Hiramoto, Y. Suzuki, A. Ali, S. Aoki, L. Berns, T. Fukuda, Y. Hanaoka, Y. Hayato, A. K. Ichikawa, H. Kawahara *et al.* (NINJA Collaboration), *First measurement of  $\bar{\nu}_\mu$  and  $\nu_\mu$  charged-current inclusive interactions on water using a nuclear emulsion detector*, *Phys. Rev. D* **102**, 072006 (2020).
- [107] T. Fukuda *et al.*, *First neutrino event detection with nuclear emulsion at J-PARC neutrino beamline*, *Prog. Theor. Exp. Phys.* **2017**, 063C02 (2017).
- [108] K. Abe *et al.* (T2K Collaboration), *T2K ND280 Upgrade*, Technical Design Report No. CERN-SPSC-2019-001 (SPSC-TDR-006), arXiv:1901.03750.
- [109] Aaron S. Meyer, André Walker-Loud, and Callum Wilkinson, *Status of lattice QCD determination of nucleon form factors and their relevance for the few-GeV neutrino program*, *Annu. Rev. Nucl. Part. Sci.* **72**, 205 (2022).
- [110] Teppei Katori and Marco Martini, *Neutrino-nucleus cross sections for oscillation experiments* (2016).
- [111] L. Alvarez Ruso *et al.*, *Theoretical tools for neutrino scattering: interplay between lattice QCD, EFTs, nuclear physics, phenomenology, and neutrino event generators*, Reports No. DESY-22-05, No. FERMILAB-FN-1161-T, and No. MITP-22-027, arXiv:2203.09030.
- [112] K. Kodama *et al.* (DONuT Collaboration), *Final tau-neutrino results from the DONuT experiment*, *Phys. Rev. D* **78**, 052002 (2008).
- [113] N. Agafonova *et al.* (OPERA Collaboration), *OPERA tau neutrino charged current interactions*, *Sci. Data* **8**, 218 (2021).
- [114] M. G. Aartsen *et al.* (IceCube Collaboration), *Measurement of atmospheric tau neutrino appearance with IceCube DeepCore*, *Phys. Rev. D* **99**, 032007 (2019).
- [115] Z. Li *et al.* (Super-Kamiokande Collaboration), *Measurement of the tau neutrino cross section in atmospheric neutrino oscillations with Super-Kamiokande*, *Phys. Rev. D* **98**, 052006 (2018).
- [116] J. A. Formaggio and G. P. Zeller, *From eV to EeV: Neutrino cross sections across energy scales*, *Rev. Mod. Phys.* **84**, 1307 (2012).

- [117] A. Lovato, J. Carlson, S. Gandolfi, N. Rocco, and R. Schiavilla, *Ab initio study of  $(\nu_e, \ell^-)$  and  $(\bar{\nu}_e, \ell^+)$  inclusive scattering in  $^{12}\text{C}$ : Confronting the MiniBooNE and T2K CCQE data*, *Phys. Rev. X* **10**, 031068 (2020).
- [118] M. Khachatryan *et al.* (CLAS and e4v Collaborations), *Electron-beam energy reconstruction for neutrino oscillation measurements*, *Nature (London)* **599**, 565 (2021).
- [119] Omar Benhar, Patrick Huber, Camillo Mariani, and Davide Meloni, *Neutrino–nucleus interactions and the determination of oscillation parameters*, *Phys. Rep.* **700**, 1 (2017).
- [120] L. Alvarez-Ruso *et al.* (NuSTEC Collaboration), *NuSTEC white paper: Status and challenges of neutrino–nucleus scattering*, *Prog. Part. Nucl. Phys.* **100**, 1 (2018).
- [121] Kendall Mahn, Chris Marshall, and Callum Wilkinson, *Progress in measurements of 0.1–10 GeV neutrino–nucleus scattering and anticipated results from future experiments*, *Annu. Rev. Nucl. Part. Sci.* **68**, 105 (2018).
- [122] Also includes uncertainty in the tagging efficiency of neutrons from detector performance [123].
- [123] T. J. Irvine, *Development of neutron-tagging techniques and application to atmospheric neutrino oscillation analysis in Super-Kamiokande*, Ph.D. thesis, 2014.
- [124] Ilya Kravchenko, Dave Z. Besson, and Joshua E. Meyers, *In situ index-of-refraction measurements of the South Polar firn with the RICE detector*, *J. Glaciol.* **50**, 522 (2004).
- [125] M. G. Aartsen *et al.* (IceCube Collaboration), *Energy reconstruction methods in the IceCube neutrino telescope*, *J. Instrum.* **9**, P03009 (2014).
- [126] R. Abbasi *et al.*, *A convolutional neural network based cascade reconstruction for the IceCube Neutrino Observatory*, *J. Instrum.* **16**, P07041 (2021).
- [127] J. García-Méndez, N. Geißelbrecht, T. Eberl, M. Ardid, and S. Ardid (ANTARES Collaboration), *Deep learning reconstruction in ANTARES*, *J. Instrum.* **16**, C09018 (2021).
- [128] Pablo Fernández (Super-Kamiokande Collaboration), *Benefits of Gd for high energy neutrinos in SuperK-Gd*, *J. Phys. Conf. Ser.* **888**, 012054 (2017).
- [129] John F. Beacom and Mark R. Vagins, *Antineutrino spectroscopy with large water Čerenkov detectors*, *Phys. Rev. Lett.* **93**, 171101 (2004).
- [130] B. Aharmim *et al.* (SNO Collaboration), *Combined analysis of all three phases of solar neutrino data from the Sudbury Neutrino Observatory*, *Phys. Rev. C* **88**, 025501 (2013).
- [131] K. Abe *et al.* (Super-Kamiokande Collaboration), *Solar neutrino measurements in Super-Kamiokande-IV*, *Phys. Rev. D* **94**, 052010 (2016).
- [132] M. Agostini *et al.* (BOREXINO Collaboration), *Experimental evidence of neutrinos produced in the CNO fusion cycle in the Sun*, *Nature (London)* **587**, 577 (2020).
- [133] A. Gando, Y. Gando, H. Hanakago, H. Ikeda, K. Inoue, K. Ishidoshiro, H. Ishikawa, M. Koga, R. Matsuda, S. Matsuda *et al.* (KamLAND Collaboration), *Reactor on-off antineutrino measurement with KamLAND*, *Phys. Rev. D* **88**, 033001 (2013).
- [134] H. de Kerret *et al.* (Double Chooz Collaboration), *Double Chooz  $\theta_{13}$  measurement via total neutron capture detection*, *Nat. Phys.* **16**, 558 (2020).
- [135] G. Bak, J. H. Choi, H. I. Jang, J. S. Jang, S. H. Jeon, K. K. Joo, K. Ju, D. E. Jung, J. G. Kim, J. H. Kim *et al.* (RENO Collaboration), *Measurement of reactor antineutrino oscillation amplitude and frequency at RENO*, *Phys. Rev. Lett.* **121**, 201801 (2018).
- [136] Feng Peng An *et al.* (Daya Bay Collaboration), *Improved measurement of the reactor antineutrino flux and spectrum at Daya Bay*, *Chin. Phys. C* **41**, 013002 (2017).
- [137] M. A. Acero *et al.* (NO $\nu$ A), *First measurement of neutrino oscillation parameters using neutrinos and antineutrinos by NO $\nu$ A*, *Phys. Rev. Lett.* **123**, 151803 (2019).
- [138] P. Adamson *et al.* (MINOS Collaboration), *Measurement of neutrino and antineutrino oscillations using beam and atmospheric data in MINOS*, *Phys. Rev. Lett.* **110**, 251801 (2013).
- [139] M. G. Aartsen *et al.* (IceCube Collaboration), *Measurement of atmospheric neutrino oscillations at 6–56 GeV with IceCube DeepCore*, *Phys. Rev. Lett.* **120**, 071801 (2018).
- [140] S. Adrian-Martinez *et al.* (ANTARES Collaboration), *Measurement of atmospheric neutrino oscillations with the ANTARES neutrino telescope*, *Phys. Lett. B* **714**, 224 (2012).
- [141] Evgeny K. Akhmedov, Michele Maltoni, and Alexei Yu. Smirnov, *1–3 leptonic mixing and the neutrino oscillograms of the Earth*, *J. High Energy Phys.* **05** (2007) 077.
- [142] H. Nunokawa, S. Parke, and R. Zukanovich Funchal, *Another possible way to determine the neutrino mass hierarchy*, *Phys. Rev. D* **72**, 013009 (2005).
- [143] Jessica Elevant and Thomas Schwetz, *On the determination of the leptonic CP phase*, *J. High Energy Phys.* **09** (2015) 016.
- [144] A. Cervera, A. Donini, M. B. Gavela, J. J. Gomez Cadenas, P. Hernandez, Olga Mena, and S. Rigolin, *Golden measurements at a neutrino factory*, *Nucl. Phys.* **B579**, 17 (2000); **B593**, 731(E) (2001).
- [145] Martin Freund, *Analytic approximations for three neutrino oscillation parameters and probabilities in matter*, *Phys. Rev. D* **64**, 053003 (2001).
- [146] Ivan Esteban, M. C. Gonzalez-Garcia, Michele Maltoni, Thomas Schwetz, and Albert Zhou, *The fate of hints: Updated global analysis of three-flavor neutrino oscillations*, *J. High Energy Phys.* **09** (2020) 178.
- [147] Francesco Capozzi, Eleonora Di Valentino, Eligio Lisi, Antonio Marrone, Alessandro Melchiorri, and Antonio Palazzo, *Unfinished fabric of the three neutrino paradigm*, *Phys. Rev. D* **104**, 083031 (2021).
- [148] If the long-baseline measurement is combined with SuperK, the preference for NO rises to  $\Delta\chi^2 \sim 7$ .
- [149] K. J. Kelly, P. A. N. Machado, I. Martinez-Soler, S. J. Parke, and Y. F. Perez-Gonzalez, *Sub-GeV atmospheric neutrinos and CP violation in DUNE*, *Phys. Rev. Lett.* **123**, 081801 (2019).
- [150] Ivan Martinez-Soler and Hisakazu Minakata, *Perturbing neutrino oscillations around the solar resonance*, *Prog. Theor. Exp. Phys.* **2019**, 073B07 (2019).

- [151] C. Jarlskog, *Commutator of the quark mass matrices in the standard electroweak model and a measure of maximal CP nonconservation*, *Phys. Rev. Lett.* **55**, 1039 (1985).
- [152] C. Jarlskog, *A basis independent formulation of the connection between quark mass matrices, CP violation and experiment*, *Z. Phys. C* **29**, 491 (1985).
- [153] Peter B. Denton, Hisakazu Minakata, and Stephen J. Parke, *Compact perturbative expressions for neutrino oscillations in matter*, *J. High Energy Phys.* **06** (2016) 015.
- [154] At higher energies and the CP term is largely suppressed due to  $\Delta_{21}$  that goes to zero, so that  $\delta_{CP}$  has a larger impact on the neutrino evolution at sub-GeV energies and for Earth-size baselines.
- [155] The atmospheric experiments can use the electron and muon event samples to search for the CP-violation effects.
- [156] S. P. Mikheyev and A. Yu. Smirnov, *Resonance amplification of oscillations in matter and spectroscopy of solar neutrinos*, *Sov. J. Nucl. Phys.* **42**, 913 (1985), <https://inspirehep.net/literature?sort=mostrecent&size=25&page=1&q=find%20J%20%22Sov.J.Nucl.Phys.%2C42%2C913%22&ui-citation-summary=true>.
- [157] Evgeny K. Akhmedov, *Neutrino oscillations in inhomogeneous matter (in Russian)*, *Sov. J. Nucl. Phys.* **47**, 301 (1988), <https://inspirehep.net/literature?sort=mostrecent&size=250&page=1&q=Sov.%20J.%20Nucl.%20Phys.%2047%2C%20301&ui-citation-summary=true>.
- [158] S. T. Petcov, *Diffraction-like (or parametric resonance-like?) enhancement of the Earth (day-night) effect for solar neutrinos crossing the Earth core*, *Phys. Lett. B* **434**, 321 (1998).
- [159] Evgeny K. Akhmedov, *Parametric resonance of neutrino oscillations and passage of solar and atmospheric neutrinos through the earth*, *Nucl. Phys.* **B538**, 25 (1999).
- [160] Evgeny K. Akhmedov, A. Dighe, P. Lipari, and A. Y. Smirnov, *Atmospheric neutrinos at Super-Kamiokande and parametric resonance in neutrino oscillations*, *Nucl. Phys.* **B542**, 3 (1999).
- [161] M. Chizhov, M. Maris, and S. T. Petcov, *On the oscillation length resonance in the transitions of solar and atmospheric neutrinos crossing the earth core*, Report No. SISSA 53/98/EP, [arXiv:hep-ph/9810501](https://arxiv.org/abs/hep-ph/9810501).
- [162] Q. Y. Liu, S. P. Mikheyev, and A. Yu. Smirnov, *Parametric resonance in oscillations of atmospheric neutrinos?*, *Phys. Lett. B* **440**, 319 (1998).
- [163] M. V. Chizhov and S. T. Petcov, *New conditions for a total neutrino conversion in a medium*, *Phys. Rev. Lett.* **83**, 1096 (1999).
- [164] M. V. Chizhov and S. T. Petcov, *Enhancing mechanisms of neutrino transitions in a medium of nonperiodic constant density layers and in the Earth*, *Phys. Rev. D* **63**, 073003 (2001).
- [165] Tommy Ohlsson and Hakan Snellman, *Neutrino oscillations with three flavors in matter: Applications to neutrinos traversing the Earth*, *Phys. Lett. B* **474**, 153 (2000); **480**, 419(E) (2000).
- [166] Sergio Palomares-Ruiz and S. T. Petcov, *Three-neutrino oscillations of atmospheric neutrinos,  $\theta_{13}$ , neutrino mass hierarchy and iron magnetized detectors*, *Nucl. Phys.* **B712**, 392 (2005).
- [167] Evgeny K. Akhmedov, M. Maltoni, and A. Yu. Smirnov, *Oscillations of high energy neutrinos in matter: Precise formalism and parametric resonance*, *Phys. Rev. Lett.* **95**, 211801 (2005).
- [168] Raj Gandhi, Pomita Ghoshal, Srubabati Goswami, Poonam Mehta, and S. U. Sankar, *Earth matter effects at very long baselines and the neutrino mass hierarchy*, *Phys. Rev. D* **73**, 053001 (2006).
- [169] The reconstruction of that oscillation pattern has allowed IceCube-DeepCore [68] to determine those oscillation parameters with similar precision to LBL experiments.
- [170] Carlos A. Argüelles, Jordi Salvado, and Christopher N. Weaver, *NUSQUIDS: A toolbox for neutrino propagation*, *Comput. Phys. Commun.* **277**, 108346 (2022).
- [171] A. M. Dziewonski and D. L. Anderson, *Preliminary reference Earth model*, *Phys. Earth Planet. Inter.* **25**, 297 (1981).
- [172] G. L. Fogli, E. Lisi, A. Marrone, D. Montanino, and A. Palazzo, *Getting the most from the statistical analysis of solar neutrino oscillations*, *Phys. Rev. D* **66**, 053010 (2002).
- [173] Pauli Virtanen *et al.*, *SCIPY 1.0—Fundamental algorithms for scientific computing in PYTHON*, *Nat. Methods* **17**, 261 (2020).
- [174] Y. Fukuda *et al.* (Super-Kamiokande Collaboration), *The Super-Kamiokande detector*, *Nucl. Instrum. Methods Phys. Res., Sect. A* **501**, 418 (2003).
- [175] Y. Fukuda *et al.* (Super-Kamiokande Collaboration), *Evidence for oscillation of atmospheric neutrinos*, *Phys. Rev. Lett.* **81**, 1562 (1998).
- [176] K. Abe *et al.* (Super-Kamiokande Collaboration), *First gadolinium loading to Super-Kamiokande*, *Nucl. Instrum. Methods Phys. Res., Sect. A* **1027**, 166248 (2022).
- [177] K. Abe *et al.* (Super-Kamiokande Collaboration), *Solar neutrino results in Super-Kamiokande-III*, *Phys. Rev. D* **83**, 052010 (2011).
- [178] A. Renshaw *et al.* (Super-Kamiokande Collaboration), *First indication of terrestrial matter effects on solar neutrino oscillation*, *Phys. Rev. Lett.* **112**, 091805 (2014).
- [179] M. H. Ahn *et al.* (K2K Collaboration), *Measurement of neutrino oscillation by the K2K experiment*, *Phys. Rev. D* **74**, 072003 (2006).
- [180] A. Suzuki *et al.* (K2K Collaboration), *Design, construction, and operation of SciFi tracking detector for K2K experiment*, *Nucl. Instrum. Methods Phys. Res., Sect. A* **453**, 165 (2000).
- [181] K. Nitta, E. Aliu, S. Andringa, S. Aoki, S. Choi, U. Dore, X. Espinal, J. Gomezcadenas, R. Gran, and M. Hasegawa, *The K2K SciBar detector*, *Nucl. Instrum. Methods Phys. Res., Sect. A* **535**, 147 (2004).
- [182] K. Abe *et al.* (T2K Collaboration), *The T2K experiment*, *Nucl. Instrum. Methods Phys. Res., Sect. A* **659**, 106 (2011).
- [183] Y. Itow *et al.* (T2K Collaboration), *The JHF-Kamioka neutrino project*, Reports No. KEK report 2001-4, No. ICRR-report-477-2001-7, and No. TRI-PP-01-05, [arXiv:hep-ex/0106019](https://arxiv.org/abs/hep-ex/0106019).
- [184] K. Abe *et al.* (T2K Collaboration), *T2K measurements of muon neutrino and antineutrino disappearance using  $3.13 \times 10^{21}$  protons on target*, *Phys. Rev. D* **103**, L011101 (2021).

- [185] K. Abe *et al.* (T2K Collaboration), *Improved constraints on neutrino mixing from the T2K experiment with  $3.13 \times 10^{21}$  protons on target*, *Phys. Rev. D* **103**, 112008 (2021).
- [186] R. Wendell *et al.* (Super-Kamiokande Collaboration), *Atmospheric neutrino oscillation analysis with sub-leading effects in Super-Kamiokande I, II, and III*, *Phys. Rev. D* **81**, 092004 (2010).
- [187] K. Abe *et al.* (Super-Kamiokande Collaboration), *Test of Lorentz invariance with atmospheric neutrinos*, *Phys. Rev. D* **91**, 052003 (2015).
- [188] K. Abe *et al.* (Super-Kamiokande Collaboration), *Limits on sterile neutrino mixing using atmospheric neutrinos in Super-Kamiokande*, *Phys. Rev. D* **91**, 052019 (2015).
- [189] M. Jiang *et al.* (Super-Kamiokande Collaboration), *Atmospheric neutrino oscillation analysis with improved event reconstruction in Super-Kamiokande IV*, *Prog. Theor. Exp. Phys.* **2019**, 053F01 (2019).
- [190] Costas Andreopoulos, Christopher Barry, Steve Dytman, Hugh Gallagher, Tomasz Golan, Robert Hatcher, Gabriel Perdue, and Julia Yarba, *The GENIE neutrino Monte Carlo generator: Physics and user manual*, arXiv:1510.05494.
- [191] Mark Vagins, *Solar/dsnb neutrino sk-gd* (2022).
- [192] Pablo Fernandez Menendez (Super-Kamiokande Collaboration), *Atmospheric neutrino oscillations with Super-Kamiokande and prospects for SuperK-Gd*, *Proc. Sci., ICRC2021* (2021) 008.
- [193] J. Bian, F. Di Lodovico, S. Horiuchi, J. G. Learned, C. Mariani, J. Maricic, J. Pedro Ochoa Ricoux, C. Rott, M. Shiozawa, M. B. Smy, H. W. Sobel, and R. B. Vogelaar, *Hyper-Kamiokande experiment: A Snowmass white paper*, arXiv:2203.02029.
- [194] Jeanne Wilson, *Accelerator neutrino ii\_hyper-k* (2022).
- [195] Shota Izumiyama, *Evaluation of neutron tagging performance in the Hyper-Kamiokande experiment*, *J. Phys. Conf. Ser.* **2156**, 012204 (2021).
- [196] Sergio Luis Suarez Gomez and Pablo Fernandez Menendez, *New approaches of first selection for neutron tagging in Hyper-Kamiokande*, *Proc. Sci., NuFact2021* (2022) 241.
- [197] A. Achterberg *et al.* (IceCube Collaboration), *First year performance of the IceCube Neutrino Telescope*, *Astropart. Phys.* **26**, 155 (2006).
- [198] M. G. Aartsen *et al.* (IceCube Collaboration), *Development of an analysis to probe the neutrino mass ordering with atmospheric neutrinos using three years of IceCube DeepCore data*, *Eur. Phys. J. C* **80**, 9 (2020).
- [199] Aya Ishihara (IceCube Collaboration), *The IceCube upgrade—Design and science goals*, *Proc. Sci., ICRC2019* (2021) 1031 [arXiv:1908.09441].
- [200] Tom Stuttard (IceCube Collaboration), *Neutrino oscillations and PMNS unitarity with IceCube/DeepCore and the IceCube upgrade*, *Proc. Sci., NuFact2019* (2020) 099.
- [201] IceCube Collaboration, *IceCube upgrade neutrino Monte Carlo simulation* (2020).
- [202] S. Adrian-Martinez *et al.* (KM3Net Collaboration), *Letter of intent for KM3NeT 2.0*, *J. Phys. G* **43**, 084001 (2016).
- [203] S. Aiello *et al.* (KM3NeT Collaboration), *Determining the neutrino mass ordering and oscillation parameters with KM3NeT/ORCA*, *Eur. Phys. J. C* **82**, 26 (2022).
- [204] D. Adey *et al.* (Daya Bay Collaboration), *Measurement of the electron antineutrino oscillation with 1958 days of operation at Daya Bay*, *Phys. Rev. Lett.* **121**, 241805 (2018).
- [205] Jeff Hartnell, *Accelerator neutrino INOνA* (2022).
- [206] F. Capozzi, E. Lisi, A. Marrone, and A. Palazzo, *Current unknowns in the three neutrino framework*, *Prog. Part. Nucl. Phys.* **102**, 48 (2018).
- [207] Kevin J. Kelly, Pedro A. N. Machado, Stephen J. Parke, Yuber F. Perez-Gonzalez, and Renata Zukanovich Funchal, *Neutrino mass ordering in light of recent data*, *Phys. Rev. D* **103**, 013004 (2021).
- [208] Christophe Bronner, *Accelerator neutrino I\_Recent results from T2K* (2022).
- [209] K. S. Babu, Chung Ngoc Leung, and James T. Pantaleone, *Renormalization of the neutrino mass operator*, *Phys. Lett. B* **319**, 191 (1993).
- [210] Piotr H. Chankowski and Zbigniew Pluciennik, *Renormalization group equations for seesaw neutrino masses*, *Phys. Lett. B* **316**, 312 (1993).
- [211] Ferruccio Feruglio, Paride Paradisi, and Andrea Pattori, *On the importance of electroweak corrections for B anomalies*, *J. High Energy Phys.* **09** (2017) 061.
- [212] Juan Carlos Criado and Ferruccio Feruglio, *Modular invariance faces precision neutrino data*, *SciPost Phys.* **5**, 042 (2018).
- [213] P. P. Novichkov, J. T. Penedo, S. T. Petcov, and A. V. Titov, *Generalised CP symmetry in modular-invariant models of flavour*, *J. High Energy Phys.* **07** (2019) 165.
- [214] K. S. Babu, Vedran Brdar, André de Gouvêa, and Pedro A. N. Machado, *Energy-dependent neutrino mixing parameters at oscillation experiments*, *Phys. Rev. D* **105**, 115014 (2022).
- [215] Ivan Martinez-Soler and Hisakazu Minakata, *Measuring tau neutrino appearance probability via unitarity*, *Phys. Rev. D* **104**, 093006 (2021).
- [216] Peter B. Denton, *Tau neutrino identification in atmospheric neutrino oscillations without particle identification or unitarity*, *Phys. Rev. D* **104**, 113003 (2021).
- [217] P. de Perio, *Progress on analysis technologies for the Hyper-Kamiokande water Cherenkov detectors* (2022).